

MICROCOPY RESOLUTION TEST CHART
NATIONAL BUREAU OF STANDARDS-1963-A

①



Waves Which Travel Upstream in Boundary Layers

Harold I. Rogler
United Research Corporation
428 Hill Street, Suite 21
Santa Monica, California 90405

July 1985

Final Report for Period March 1982 – August 1984

Approved for public release; distribution unlimited.

AD-A157 949

DTIC FILE COPY

DTIC
ELECTE
AUG 15 1985
S D

**ARNOLD ENGINEERING DEVELOPMENT CENTER
ARNOLD AIR FORCE STATION, TENNESSEE
AIR FORCE SYSTEMS COMMAND
UNITED STATES AIR FORCE**

85 8 9 088

NOTICES
When U. S. Government drawings, specifications, or other data are used for any purpose other than a definitely related Government procurement operation, the Government thereby incurs no responsibility nor any obligation whatsoever, and the fact that the government may have formulated, furnished, or in any way supplied the said drawings, specifications, or other data, is not to be regarded by implication or otherwise, or in any manner licensing the holder or any other person or corporation, or conveying any rights or permission to manufacture, use, or sell any patented invention that may in any way be related thereto.
Qualified users may obtain copies of this report from the Defense Technical Information Center.
References to named commercial products in this report are not to be considered in any sense as an endorsement of the product by the United States Air Force or the Government.

This final report was submitted by United Research Corporation, Santa Monica, California 90405, under contract F40600-7-C-0002, with Arnold Engineering Development Center, Air Force Systems Command, Arnold Air Force Station, TN 37389-5000. Mr. Keith Kushman was the AEDC Project Manager. The reproducibles used in the reproduction of this report were supplied by the author.

APPROVAL STATEMENT

This report has been reviewed and approved.



KEITH L. KUSHMAN
Directorate of Technology
Deputy for Operations

Approved for publication:

FOR THE COMMANDER



MARION L. LASTER
Director of Technology
Deputy for Operations

UNCLASSIFIED

AD-A157949

SECURITY CLASSIFICATION OF THIS PAGE

REPORT DOCUMENTATION PAGE				
1a REPORT SECURITY CLASSIFICATION UNCLASSIFIED		1b. RESTRICTIVE MARKINGS		
2a SECURITY CLASSIFICATION AUTHORITY		3 DISTRIBUTION AVAILABILITY OF REPORT		
2b DECLASSIFICATION/DOWNGRADING SCHEDULE		Approved for public release; distribution unlimited.		
4 PERFORMING ORGANIZATION REPORT NUMBER(S) AEDC-TR-83-7		5 MONITORING ORGANIZATION REPORT NUMBER(S)		
6a NAME OF PERFORMING ORGANIZATION United Research Corporation		6b OFFICE SYMBOL (If applicable)	7a NAME OF MONITORING ORGANIZATION	
6c ADDRESS (City, State and ZIP Code) 428 Hill Street, Suite 21 Santa Monica, California 90405		7b ADDRESS (City, State and ZIP Code)		
8a NAME OF FUNDING/SPONSORING ORGANIZATION Arnold Engineering Development Center		8b OFFICE SYMBOL (If applicable) 00	9. PROCUREMENT INSTRUMENT IDENTIFICATION NUMBER F40600-79-C-0002	
8c ADDRESS (City, State and ZIP Code) Air Force Systems Command Arnold Air Force Station, TN 37389-5000		10. SOURCE OF FUNDING NOS		
11 TITLE (Include Security Classification) See Reverse of This Page.		PROGRAM ELEMENT NO	PROJECT NO.	TASK NO
		65807F		WORK UNIT NO
12 PERSONAL AUTHOR(S) Rogler, Harold L., United Research Corporation				
13a. TYPE OF REPORT Final	13b. TIME COVERED FROM 3/82 TO 8/84	14 DATE OF REPORT (Yr., Mo., Day) July 1985	15. PAGE COUNT 57	
16 SUPPLEMENTARY NOTATION Available in Defense Technical Information Center (DTIC).				
17 COSATI CODES		18. SUBJECT TERMS (Continue on reverse if necessary and identify by block number)		
FIELD	GROUP	SUB GR.	upstream-traveling waves; Chebyshev polynomials	
20	04		upstream diffusion; Orr-Sommerfeld equation	
20	03		unsteady boundary layers. (Cont)	
19. ABSTRACT (Continue on reverse if necessary and identify by block number) Upstream propagation and diffusion of vorticity in a boundary layer is described by a numerical solution of the Orr-Sommerfeld equation. This traveling wave grows very rapidly in the downstream direction. The growth rate is approximately $\exp(+R_\delta x)$, where R_δ is the Reynolds number based on the characteristic boundary layer thickness, and x is the streamwise coordinate nondimensionalized against δ . Far from the boundary layer, the solution oscillates neutrally in the y -direction. Analyses reveal a high-frequency wave which oscillates and decays in the y -direction approximately as $\exp(-iR_\delta y - \omega y)$ where ω is the frequency. This high frequency wave can survive into the freestream. Numerical solutions of the Orr-Sommerfeld equation with a Blasius layer are obtained by a series expansion of Chebyshev polynomials. Since the y -wavenumber of the oscillations increases with increasing Reynolds number, the calculations have been restricted to low Reynolds numbers. In the boundary-value problem, this solution appears as a branch line in (Cont)				
20 DISTRIBUTION AVAILABILITY OF ABSTRACT UNCLASSIFIED/UNLIMITED <input type="checkbox"/> SAME AS RPT <input checked="" type="checkbox"/> DTIC USERS <input type="checkbox"/>		21 ABSTRACT SECURITY CLASSIFICATION UNCLASSIFIED		
22a NAME OF RESPONSIBLE INDIVIDUAL W. O. Cole		22b TELEPHONE NUMBER (Include Area Code) (615)455-2611 Ext. 7813	22c OFFICE SYMBOL DOS	

DD FORM 1473, 83 APR

EDITION OF 1 JAN 73 IS OBSOLETE

UNCLASSIFIED
SECURITY CLASSIFICATION OF THIS PAGE

UNCLASSIFIED

SECURITY CLASSIFICATION OF THIS PAGE

11. TITLE

Waves Which Travel Upstream in Boundary Layers

18. SUBJECT TERMS (Concluded)

mathematical completeness;
numerical boundary conditions;
growing solutions;
stability;
transition

19. ABSTRACT (Concluded)

Laplace space. It is one of the possible solutions in a mathematically complete description of the spatial evolution of fluctuations. This traveling wave represents one of the upstream influences of a boundary in a calculational domain. Another mechanism of upstream influence is the growing standing wave.

SEARCHED		INDEXED	
SERIALIZED		FILED	
MAR 1968			
FBI - MEMPHIS			
By _____			
Distribution/			
Availability Codes			
Dist.	Avail. and/or	Special	
AI			

UNCLASSIFIED

SECURITY CLASSIFICATION OF THIS PAGE



PREFACE

This research is supported by the Arnold Engineering Development Center of the Air Force Systems Command under Contract F40600-79-C-0002. Dr. Keith Kushman is the Technical Monitor. Mrs. Ernestine Badman is the Contracting Officer.

This report was drafted in March 1982 and summarized at an Air Force Boundary Layer Transition Study Group meeting. I thank the members of that committee for their constructive comments, and thank Dr. Kushman for his review of this report. I also thank Mr. Chih-Tsai Chen (United Research Corporation) for assistance with several plotting programs.

This report is part of a series of AEDC Technical Reports and papers which describe the solutions of the Orr-Sommerfeld and Rayleigh equations and how these fluctuations are generated. These reports and papers are:

AEDC-TR-83-3

Rotational and Irrotational Freestream Disturbances
Interacting Inviscidly with a Semi-Infinite Plate
by Harold L. Rogler and Eli Reshotko, April 1983

AEDC-TR-83-4

Exponentially-Varying, Unsteady Standing Waves
in Parallel-Flow Boundary Layers
by Harold L. Rogler, May 1983

Related AIAA paper: Preprint 83-0045

Unsteady, Exponentially-Varying Standing Waves in Boundary Layers
AIAA 21st Aerospace Sciences Meeting, Reno, Nevada (10-13 January 1983)
(Includes a 16mm movie made with the assistance of Mr. Arnie Rosner)

AEDC-TR-83-10

Nonperiodic Fluctuations Induced by Stationary Surface Waviness
on a Semi-Infinite Plate
by Harold L. Rogler and Chih-Tsai Chen, July 1983

AEDC-TR-83-7

Waves Which Travel Upstream in Boundary Layers (this report)
by Harold L. Rogler, August 1984

AEDC-TR-84-

The Boundary-Value Problem

for Two-Dimensional Fluctuations in Boundary Layers
by Shunichi Tsuge' and Harold L. Rogler, September 1984

Related AIAA paper: Preprint 83-0044

The Two-Dimensional, Viscous Boundary-Value Problem
for Fluctuations in Boundary Layers

AIAA 21st Aerospace Sciences Meeting, Reno, Nevada (10-13 January 1983)

AEDC-TR-84-

Spatially-Decaying Arrays of Rectangular Vortices
Interacting with Falkner-Skan Boundary Layers
by Harold L. Rogler

This document is the final report on work performed by United Research Corporation, Santa Monica, California, under Contract F40600-7-C-0002 with Arnold Engineering Development Center, United States Air Force Systems Command during the period March 1982 through August 1984. The AEDC Project Manager was Keith Kushman, and the manuscript was submitted for publication on June 28, 1985.

The reproducibles used in the reproduction of this report were supplied by the authors.

TABLE OF CONTENTS

1. Introduction and Literature Survey	7
1.1 Introductory comments on the upstream traveling wave.....	7
1.2 Why study the Fourier-Laplace solutions of the Orr-Sommerfeld equation?.....	8
1.3 2-D waves diffusing upstream in the freestream	10
1.4 3-D waves diffusing upstream in a uniform flow	12
1.5 Waves propagating upstream in a uniform mean flow near a wall	14
2. Formulation of the Mathematical System for 3-D Fluctuations Interacting with Boundary Layers	24
3. Numerical Solutions for Waves Traveling Upstream in Boundary Layers	26
3.1 Summary of the numerical techniques	26
3.2 Numerical results for upstream traveling waves in a Blasius boundary layer	27
4. Summary, Discussion and Conclusions	45
4.1 Introductory comments	45
4.2 Summary of the formulation and numerical technique	46
4.3 Summary of Results, Discussion and Conclusions	48
REFERENCES	50

LIST OF FIGURES

- Figure 1.1 Envelopes for the inviscid and viscous cases of fluctuating vorticity input along the y-axis.....11
- Figure 1.2 Explicit solution for the normal velocity fluctuation for $\beta = \omega = 0.5$, $\gamma = 0$, $R_\delta = 10$ and a uniform mean flow. The variables and parameters are nondimensionalized against the dummy length δ so that the results can be compared with the calculations with a Blasius layer.....15
- Figure 1.3 Explicit solution for the longitudinal velocity fluctuation for $\beta = \omega = 0.5$, $\gamma = 0$, $R_\delta = 10$ and a uniform mean flow. The effect of Reynolds number on the high frequency oscillation can be seen by comparing this figure with Figure 1.8.....17
- Figure 1.4 Explicit solution for the vorticity fluctuation for $\beta = \omega = 0.5$, $\gamma = 0$, $R_\delta = 10$ and a uniform mean flow. The high frequency oscillations in Figures 1.2 and 1.3 do not appear here because the high-frequency oscillations are irrotational when the flow is uniform.....19
- Figure 1.5 Explicit solution for the pressure fluctuation for $\beta = \omega = 0.5$, $\gamma = 0$, $R_\delta = 10$ and a uniform mean flow.....20
- Figure 1.6 Streamlines of the fluctuating flow for $\beta = \omega = 0.5$, $\gamma = 0$, $R_\delta = 10$ and a uniform mean flow. The x-coordinate is greatly stretched to show details. The y-scale is the same as for the other figures.....21
- Figure 1.7 Equi-vorticity contours of the fluctuating flow for $\beta = \omega = 0.5$, $\gamma = 0$, $R_\delta = 10$ and a uniform mean flow. The x-coordinate is greatly stretched to show details. The high-frequency waves of Figure 1.6 do not appear in the equi-vorticity contours when the flow is uniform.....22
- Figure 1.8 Explicit solution for the longitudinal velocity fluctuation for $\beta = \omega = 0.5$, $\gamma = 0$, $R_\delta = 20$ and a uniform mean flow. This figure can be compared with Figure 1.3 to see the effect of Reynolds number on the high frequency oscillation.....23
- Figure 3.1 The mean velocity profile and derivatives for a Blasius boundary layer.....28
- Figure 3.2 Calculation of the normal velocity fluctuation for $\beta = \omega = 0.5$, $\gamma = 0$, $R_\delta = 10$ and a Blasius boundary layer. This figure (for a Blasius layer) can be compared with Figure 1.2 (for a uniform mean flow).....29
- Figure 3.3 Calculation of the rms normal velocity fluctuation for $\beta = \omega = 0.5$, $\gamma = 0$, $R_\delta = 10$ and a Blasius boundary layer.....30

Figure 3.4	Calculation of the longitudinal velocity fluctuation for $\beta = \omega = 0.5$, $\gamma = 0$, $R_\delta = 10$ and a Blasius boundary layer. This figure (for a Blasius layer) can be compared with Figure 1.3 (for a uniform mean flow).....	31
Figure 3.5	Calculation of the rms longitudinal velocity fluctuation for $\beta = \omega = 0.5$, $\gamma = 0$, $R_\delta = 10$ and a Blasius boundary layer.....	33
Figure 3.6	Streamlines of the fluctuating flow for $\beta = \omega = 0.5$, $\gamma = 0$, $R_\delta = 10$ and a Blasius boundary layer. The x-coordinate is greatly stretched to show details. The grid is 50x by 100y.....	34
Figure 3.7	Calculation of the vorticity fluctuation for $\beta = \omega = 0.5$, $\gamma = 0$, $R_\delta = 10$ and a Blasius boundary layer. This figure (for a Blasius layer) can be compared with Figure 1.4 (for a uniform mean flow). Note the appearance of high frequency rotational oscillations when the boundary layer is present.....	35
Figure 3.8	Calculation of the rms vorticity fluctuation for $\beta = \omega = 0.5$, $\gamma = 0$, $R_\delta = 10$ and a Blasius boundary layer.....	36
Figure 3.9	Calculation of the production of fluctuating vorticity for $\beta = \omega = 0.5$, $\gamma = 0$, $R_\delta = 10$ and a Blasius boundary layer. This term vanishes for a uniform mean flow.....	37
Figure 3.10	Contours of equi-vorticity for $\beta = \omega = 0.5$, $\gamma = 0$, $R_\delta = 10$ and a Blasius boundary layer. This figure with a Blasius layer can be compared with Figure 1.7 with a uniform mean flow.....	38
Figure 3.11	Calculation of the fluctuating pressure for $\beta = \omega = 0.5$, $\gamma = 0$, $R_\delta = 10$ and a Blasius boundary layer. This figure (for a Blasius layer) can be compared with Figure 1.5 (for a uniform mean flow).....	39
Figure 3.12	Calculation of the rms fluctuating pressure for $\beta = \omega = 0.5$, $\gamma = 0$, $R_\delta = 10$ and a Blasius boundary layer.....	40
Figure 3.13	Calculation of Reynolds stress for $\beta = \omega = 0.5$, $\gamma = 0$, $R_\delta = 10$ and a Blasius boundary layer.....	41
Figure 3.14	Calculation of the energy production for $\beta = \omega = 0.5$, $\gamma = 0$, $R_\delta = 10$ and a Blasius boundary layer.....	42
Figure 3.15	Calculation of the disturbance kinetic energy for $\beta = \omega = 0.5$, $\gamma = 0$, $R_\delta = 10$ and a Blasius boundary layer.....	44

LIST OF TABLES

Table I.	Spatial, Fourier/Laplace Solutions for a Boundary Layer.....	9
Table II.	x-Wavenumbers and Phase Speeds for Upstream Traveling Waves.....	14

1. INTRODUCTION AND LITERATURE SURVEY

1.1 INTRODUCTORY COMMENTS ON THE UPSTREAM TRAVELING WAVE

In a spatial boundary-value problem with vorticity introduced along a grid in the freestream, Rogler and Reshotko (Ref. 1) found an explosively growing solution that represents vorticity diffusing upstream. The solution is not an eigenmode. It oscillates neutrally in the direction perpendicular to the freestream rather than vanishing far-away.

The counterpart to this solution appears in the spatial boundary-value analyses of Refs. 2-7 (for 2-D fluctuations) and Ref. 8 (for 3-D fluctuations) as a branch line. The corresponding Fourier-Laplace solution for the velocity of form $\phi(y)\exp[i\alpha x - i\omega t]$ has a complex wavenumber, $\alpha = \alpha_r + i\alpha_i$ (with α_i very large and negative, indicating rapid growth), and a real frequency, ω . It represents a third class of growing solutions of the Orr-Sommerfeld equation. This solution appears to have no counterpart in the viscous temporal initial-value formulations (Refs. 9 and 10) with α real and ω complex. Neither does it appear in the inviscid spatial solution of Ref. 11.

The other two classes of growing, spatial solutions include the Tollmien-Schlichting (T-S) wave, which is the fundamental eigenmode that can be unstable or stable depending on the parameters and boundary layer. Although there are other eigenmodes, Mack (Ref. 12) demonstrated that the higher temporal eigenmodes are finite in number and heavily damped for the Blasius layer.

Another growing solution is a standing wave. It does not travel, but grows exponentially in the streamwise direction and oscillates in time as $\exp[i\beta x - i\omega t]$ with β real. The phase speed is pure imaginary. The standing wave has been described in Refs. 13 and 14; a movie was made to visualize its behavior. The broader picture of the five spatial classes of solutions is presented in the next section.

For high Reynolds numbers, the upstream traveling wave is very difficult to calculate because of extremely high frequency oscillations in the solutions. The high frequency oscillation for the upstream traveling wave has a y-wavenumber $O(R_\delta)$, as compared with $O(R_\delta^{1/2})$ for the T-S wave. At $R_\delta = 2500$, this wavenumber is fifty times greater than for the T-S wave.

Also, these oscillations can decay very slowly away from the wall, with a decay rate $O(\omega)$ rather than $O(R_\delta^{1/2})$ for the instability wave. That means that the high frequency oscillation can survive far from the wall for the upstream traveling wave. In contrast, the viscous solution for the T-S wave is significant only near the wall (where it represents the viscous sublayer) and the critical layer.

For these reasons, the present calculations have been restricted to low Reynolds numbers. At high Reynolds numbers, this solution will be a challenge for future developments in numerical solutions of differential equations.

Our objectives here are to describe solutions of the Orr-Sommerfeld equation for upstream traveling vorticity. Three cases are described:

- (1) Analytical solutions for vorticity in a uniform flow far from any wall (Sections 1.3,1.4)
- (2) Analytical solutions for vorticity in a uniform flow near a wall (Section 1.5)
- (3) Numerical solutions of the Orr-Sommerfeld equation for boundary layers (Chapters 2 and 3)

We believe that closely related waves traveling upstream also appear in free-shear layers, jets, wakes and other shear layers.

1.2 WHY STUDY THE FOURIER-LAPLACE SOLUTIONS OF THE ORR-SOMMERFELD EQUATION?

To accurately simulate boundary layer transition in test facilities, the processes leading to transition must be known and controlled. To understand, calculate, measure and control boundary layer transition and mixing in shear layers, it is important to identify all possible Fourier-Laplace solutions of the viscous, parallel-flow, linear equations. More sophisticated equations exist, but the importance of these equations cannot be denied. They can describe many basic phenomena in shear layers. To have a mathematically complete set of solutions which could be superimposed to satisfy appropriate upstream and downstream boundary conditions would be a practically useful accomplishment. Perhaps most importantly, even after more than 70 years since the original derivations by Orr and Sommerfeld, and after more than 50 years since the first solution by Tollmien, basic features continue to be discovered from the equations for viscous, linear, parallel-flows.

Apart from the usefulness of a complete set of solutions in initial-value problems, it is also important to be aware of physical phenomena, to be able to categorize them, and to be able to describe them physically. The Fourier-Laplace solutions help sort out these basic features.

While reasons for seeking the Fourier-Laplace solutions are summarized above, a few statements concerning what these solutions are NOT are also warranted. In many cases, a superposition of members of one family of waves or several families of waves is required. The behavior observed can be unlike that of any one Fourier component, even though that Fourier component is imbedded within the observed behavior. Secondly, nonparallelism and nonlinearity can introduce other significant features into the problems. Yet even for these cases, the Fourier-Laplace solutions based on the viscous, parallel-flow equations provide (1) the solutions which can be superimposed and (2) solutions serving as a point of departure for weak nonparallelism and weak nonlinearity.

Section 1 of Ref. 3 surveys the temporal and spatial initial-value and boundary-value problems. Section 1.6 of Ref. 14 lists the known Fourier-Laplace solutions of the Orr-Sommerfeld equation and the other viscous, parallel-flow, linear equations for incompressible flow.

The five classes of 2-D spatial solutions, including decaying ones, are tabulated in Table I below. For simplicity, the table has been restricted to

2-D fluctuations (with u and v velocities, but no w velocity) and a flat plate. However, the pattern of solutions appears to generally repeat itself for 3-D fluctuations, i.e. the poles and branch lines from 2-D formulations appear to have generalized counterparts for 3-D studies. These generalizations include longitudinal vortices and at least three other structures.

Table I has three columns: for decaying, neutral, and growing solutions in the streamwise direction. Row 1 is composed of the set of eigensolutions which vanish far away from the boundary layer. The fundamental instability wave (the Tollmien-Schlichting wave) can be unstable. As indicated by the arrows, it also can be neutral or stable depending on the parameters and boundary layer.

Row 1.2 is a pair of solutions which are vortical fluctuations in the freestream. However, 1.2a consists of vortical disturbances propagating downstream. They are summarized in Section 1.6 of Ref. 14 and will not be surveyed here. Although the details of the solutions depend on the problem considered, these vortical solutions appear in uniform flows, shearing flows, inviscid and viscous flows, and in both spatial and temporal analyses.

Solution 1.2b consists of vortical disturbances propagating upstream and growing very rapidly in the streamwise direction. Fluctuations 1.2b are described in this report.

The last row also consists of a pair of solutions, one which decays and another which grows. These two solutions are standing waves (they do not travel in the streamwise direction) and are irrotational fluctuations far away from the boundary layer. These two standing wave solutions are described in Refs. 13 and 14.

Table I
SPATIAL, FOURIER/LAPLACE SOLUTIONS FOR A BOUNDARY LAYER
of form $fct(y)\exp(iax - i\omega t)$
for viscous, incompressible, constant transport property, parallel-flow
over a stationary flat plate

Decaying in the downstream direction ←	Neutral in the streamwise direction ←	Growing in the downstream direction
		(1.1a) Tollmien-Schlichting wave
(1.1b) Higher discrete modes		
(1.2a) Downstream propagating freestream vortices		(1.2b) Upstream propagating vorticity (described in this report)
(1.3a) Decaying standing waves		(1.3b) Growing standing wave

1.3 2-D WAVES DIFFUSING UPSTREAM IN THE FREESTREAM

The Rogler-Reshotko analysis of Ref. 1 is an boundary-value problem for vorticity fluctuations in the freestream. Since this analysis illustrates four classes of solutions in Table I (but not the eigenmodes) with elementary mathematics, this analysis is summarized in this section.

The two-dimensional equation for vorticity fluctuations in a uniform flow is

$$\xi_t + \xi_x - \varepsilon(\xi_{xx} + \xi_{yy}) = 0 \tag{1.1}$$

where ε is the inverse Reynolds number. A generalized Fourier transform in the y -direction and time yields the following equation describing the evolution of vorticity in the streamwise direction

$$\varepsilon \frac{d^2 \hat{\xi}(x)}{dx^2} - \frac{d \hat{\xi}(x)}{dx} + (i\omega - \varepsilon\beta^2) \hat{\xi} = 0 \tag{1.2}$$

Seeking a solution of form $\hat{\xi}(x) = \exp(mx)$, then the characteristic equation is

$$\varepsilon m^2 - m + (i\omega - \varepsilon\beta^2) \xi = 0 \tag{1.3}$$

with solutions

$$m_{1,2} = \{1 \mp [1 - 4\varepsilon(i\omega - \varepsilon\beta^2)]^{1/2}\} / 2\varepsilon \tag{1.4}$$

Hence the complementary solution is

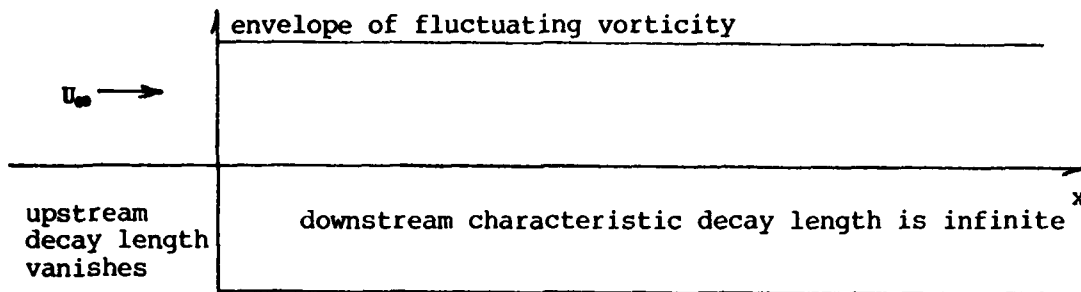
$$\hat{\xi}(x, \beta, \omega) = C_1 \exp(m_1 x) + C_2 \exp(m_2 x) \tag{1.5}$$

The first solution represents fluctuating vorticity which convects and decays in the streamwise direction. The second solution grows exponentially in the streamwise direction. Both solutions can be physically meaningful.

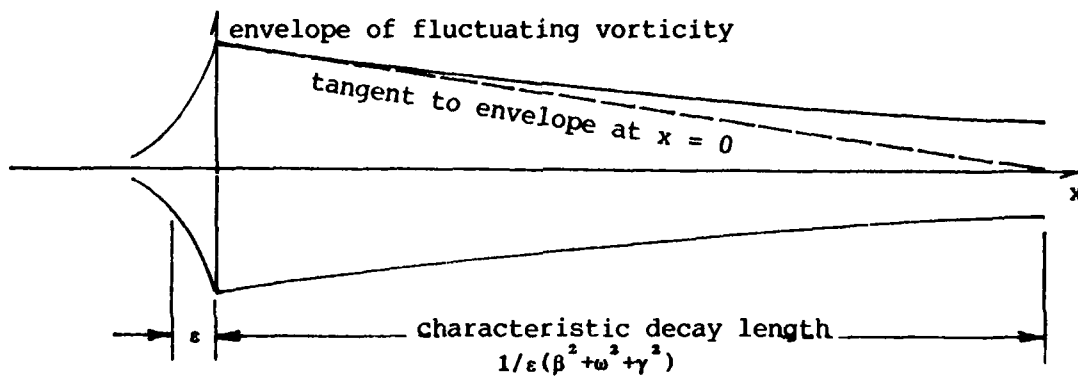
If an initial-value problem were solved for the region upstream of the y -axis, then the first solution would be discarded and the second solution retained. For the region downstream of the y -axis where the vorticity is specified, then the first solution would be retained and the second solution is discarded. If a rectangular strip were considered, then both solutions could exist in the same domain.

The inviscid and viscous solutions are sketched in Figure 1.1. Without viscosity, vorticity cannot diffuse upstream. The solution is identically zero until the fluid crosses the y -axis where the vorticity is introduced. The vorticity is convected downstream without decay.

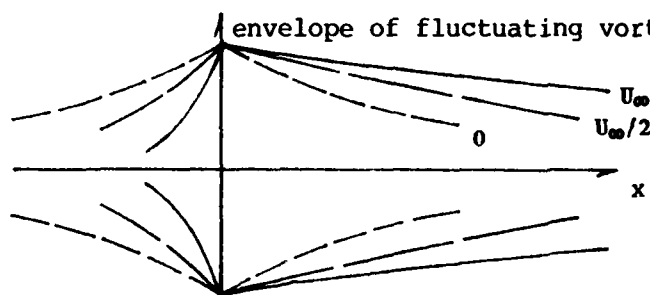
With viscosity, however, vorticity can diffuse in the upstream direction. Instead of the (inviscid) Heaviside distribution, two exponential functions



1.1a Inviscid case with a uniform mean flow



1.1b Viscous case with a uniform mean flow



1.1c Effects of reducing the mean velocity while holding the dimensional frequency and y- and z-wavenumbers constant.

Figure 1.1 Envelopes for the inviscid and viscous cases of fluctuating vorticity input along the y-axis.

join at the y -axis. The decay in the upstream direction is "very rapid", since the vorticity must diffuse upstream against the mean flow. In the downstream direction, the decay is "slow" as the vortices are convected downstream and diffuse.

Both viscous solutions may be relevant in both regions, if both positive and negative mean flows arise in both regions. An example is the case of reversed flows. Another example is the region between the leading and trailing edges of a finite-length plate.

Generalizations of the second solution to account for a boundary layer are an objective of this research.

1.4 3-D WAVES DIFFUSING UPSTREAM IN A UNIFORM FLOW

The equation describing the evolution of small-amplitude disturbances in a uniform flow ($\bar{U}=1$) reduces to

$$\left\{ \frac{\partial}{\partial t} + \frac{\partial}{\partial x} - \frac{1}{R_g} \nabla^2 \right\} v = 0 \quad (1.6)$$

Letting $v = \phi(y) \exp[i\alpha x + i\gamma z - i\omega t]$,

then the Orr-Sommerfeld equation for a uniform mean flow reduces to

$$\left[1 - \frac{\omega}{\alpha} - \frac{1}{i\alpha R_g} (D^2 - \alpha^2 - \gamma^2) \right] (D^2 - \alpha^2 - \gamma^2) \phi = 0 \quad (1.7)$$

The characteristic length δ in the nondimensionalizations is a dummy parameter for this uniform flow case. While that length could be defined as the characteristic viscous length, the same nondimensionalizations will be used here as defined in Chapter 2 so that our analytical results can be compared with the numerical solutions.

For solutions which oscillate sinusoidally in the y direction

$$\phi(y) = C \cos \beta y + D \sin \beta y \quad (1.8)$$

the Orr-Sommerfeld equation reduces to

$$\left[1 - \frac{\omega}{\alpha} + \frac{1}{i\alpha R_g} (\alpha^2 + \beta^2 + \gamma^2) \right] (\alpha^2 + \beta^2 + \gamma^2) = 0 \quad (1.9)$$

This equation has four solutions for the x -wavenumber, α . Two solutions are irrotational standing waves which grow and decay in the streamwise direction

$$\alpha = \pm i(\beta^2 + \gamma^2)^{1/2} \quad (1.10)$$

These waves are described in Ref. 13 and 14.

Two other solutions are rotational, traveling waves

$$\alpha = \frac{-iR_0}{2} \left\{ 1 - \left[1 + \frac{4}{R_0^2} (\beta^2 + \gamma^2 - i\omega R_0) \right]^{1/2} \right\} \quad (1.11a)$$

$$\alpha = \frac{-iR_0}{2} \left\{ 1 + \left[1 + \frac{4}{R_0^2} (\beta^2 + \gamma^2 - i\omega R_0) \right]^{1/2} \right\} \quad (1.11b)$$

Solution (1.11a) with the minus sign corresponds to vortical fluctuations decaying in the streamwise direction. These waves correspond to those of 1.2a in Table I. Solution (1.11b) with the positive sign is the one of interest in this report.

For large values of the Reynolds number, the series representation of the square root can be found. The results for the x -wavenumber are

$$\alpha_r = -\omega \left[1 - 2\varepsilon^2 (\beta^2 + \gamma^2 + \omega^2) + 2\varepsilon^4 (\beta^2 + \gamma^2 + \omega^2) (3\beta^2 + 3\gamma^2 + 7\omega^2) + O(\varepsilon^6) \right] \quad (1.12a)$$

$$\alpha_i = -\frac{1}{\varepsilon} - \varepsilon (\beta^2 + \gamma^2 + \omega^2) + \varepsilon^3 (\beta^2 + \gamma^2 + \omega^2) (\beta^2 + \gamma^2 + 5\omega^2) + O(\varepsilon^5) \quad (1.12b)$$

where $\varepsilon = 1/R_0$. Based on the first term of the expansion for α_i , the wave grows in the streamwise direction as

$$\exp(-\alpha_i x) = \exp(R_0 x) \quad (1.13)$$

To lowest order, this growth rate is independent of the wavenumbers and frequency. The solution for the fluctuations can be written as

$$v = \phi(\gamma) e^{-\alpha_i x} e^{i\alpha_r(x - c_{ep}t)} e^{i\gamma z} \quad (1.14)$$

where the equi-phase speed, a real quantity, is

$$c_{ep} = \omega/\alpha_r = -1 - 2\varepsilon^2 (\beta^2 + \gamma^2 + \omega^2) + 2\varepsilon^4 (\beta^2 + \gamma^2 + \omega^2) (\beta^2 + \gamma^2 + 5\omega^2) + O(\varepsilon^6) \quad (1.15)$$

This quantity is the speed of a point of constant phase on the wave, such as a local maximum or minimum, a point of zero value, etc. This speed is negative, indicating that the waves propagate upstream.

Table II tabulates a few values of wavenumber and equi-phase speed for various Reynolds numbers. In the limit as $R_\delta \rightarrow \infty$, the waves propagate at a speed equal to the freestream speed, U_∞ , in the upstream direction.

Table II

x-Wavenumbers and Phase Speeds for Upstream Traveling Waves
 $\beta = \omega = 0.5, \gamma = 0$

R_δ	α_r	α_i	$c_{ep} = \omega/\alpha_r$
1.0	-0.3217971	-1.2768869	-1.553774
10.0	-0.4951209	-10.049272	-1.0098543
100.0	-0.4999500	-100.00500	-1.0000999
1000.0	-0.4999995	-1000.0005	-1.0000010
∞	-0.5	$-R_\delta$	-1.0

1.5 WAVES PROPAGATING UPSTREAM IN A UNIFORM MEAN FLOW NEAR A WALL

Some features of waves propagating upstream near a wall can be extracted from the uniform-flow version of the Orr-Sommerfeld equation. The x-wavenumber is given by eqn. (1.11b). Seeking solutions of form $\exp(my)$, the four independent solutions are

$$\phi = Ae^{-my} + Be^{+my} + C\cos\beta y + D\sin\beta y \quad (1.16a)$$

with $B = 0, C = 1,$ and $m = (\alpha^2 + \gamma^2)^{1/2} \quad (1.16b)$

Introducing the impermeability and no-slip conditions, then $A = -1, D = -m/\beta,$ and

$$\phi(y) = -e^{-my} + \cos\beta y - \frac{m}{\beta}\sin\beta y \quad (1.17)$$

This velocity fluctuation is plotted in Figure 1.2. Note the high frequency oscillation which decays slowly away from the wall. Also note the undamped sinusoidal oscillation in the freestream.

In eqn.(1.16a), the velocity has been nondimensionalized by setting the constant $C=1$. In retrospect, the choice $D=1$ would be a better choice for large Reynolds numbers. If the right-hand side of eqn.(1.17) were multiplied by $-\beta/m$, the solution with this alternate nondimensionalization would result.

Expressions (1.16 and 1.17) are for 3-D disturbances. To obtain

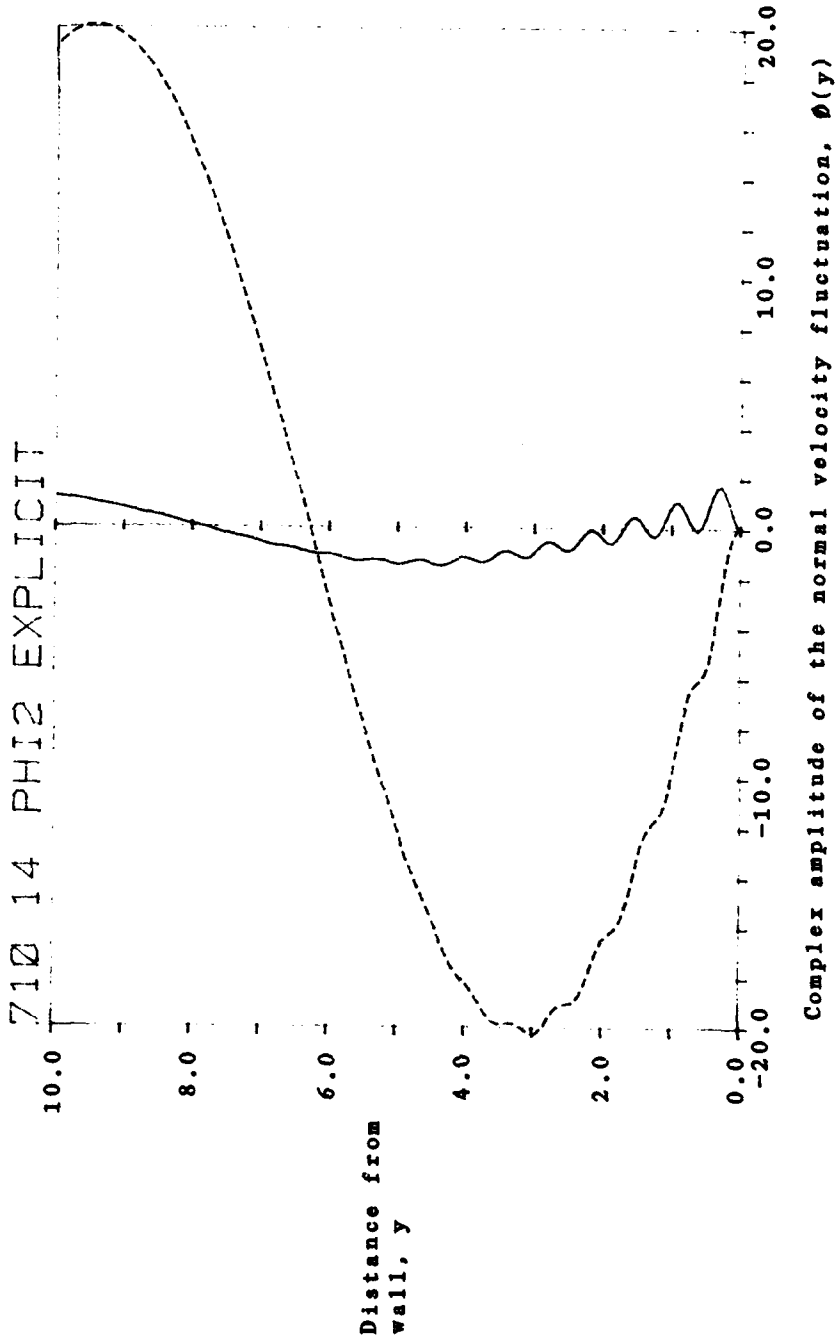


Figure 1.2 Explicit solution for the normal velocity fluctuation for $\beta = \omega = 0.5$, $\gamma = 0$, $R_6 = 10$ and a uniform mean flow. The variables and parameters are nondimensionalized against the dummy length δ so that the results can be compared with the calculations with a Blasius layer.

relations useful for comparison with the 2-D calculations in Chapter 2, the following formulae are for 2-D fluctuations.

With a positive frequency, the value of the exponent m is

$$m = -\alpha \pm \omega + iR_0 \quad (\text{for } \gamma = 0) \quad (1.18)$$

The term $\exp(-my)$ has the following approximate value for large Reynolds numbers

$$e^{-my} = e^{-iR_0 y - \omega y} \quad (\text{for } \gamma = 0) \quad (1.19)$$

Hence, the term $\exp(-my)$ can be a high y -wavenumber wave which decays slowly in the y -direction, as shown in Figure 1.2.

The longitudinal velocity

$$u = f(y)e^{i\alpha x - i\omega t} \quad (\text{for } \gamma = 0) \quad (1.20a)$$

can be found from the continuity equation, $u_x + v_y = 0$,

$$f(y) = +ie^{-my} - \frac{i\beta}{\alpha} \sin\beta y - i\cos\beta y \quad (\text{for } \gamma = 0) \quad (1.20b)$$

This amplitude is plotted in Figure 1.3 for $R_0=10$. The high frequency oscillation in $f(y)$ is proportionately much stronger than for 0. Note, however, that the scale of the abscissa has been changed. To illustrate the effect of changing Reynolds number, the amplitude $f(y)$ is plotted in Figure 1.8 for $R_0=20$. This figure clearly shows the higher frequencies associated with the term $\exp(-iR_0 y)$. While the explicit solutions of this chapter can be evaluated for much higher Reynolds numbers, the numerical solutions of the Orr-Sommerfeld equation presented in the next two chapters cannot be found for large Reynolds numbers because of the high frequency oscillation $\exp(-iR_0 y)$ which dampens slowly as $\exp(-\omega y)$ if the frequency is small. For this reason, all plots and the numerical calculations have been restricted to low Reynolds numbers.

From the definition of vorticity,

$$\zeta = v_x - u_y = Z(y)e^{i\alpha x - i\omega t} \quad (\text{for } \gamma = 0) \quad (1.21a)$$

the amplitude is

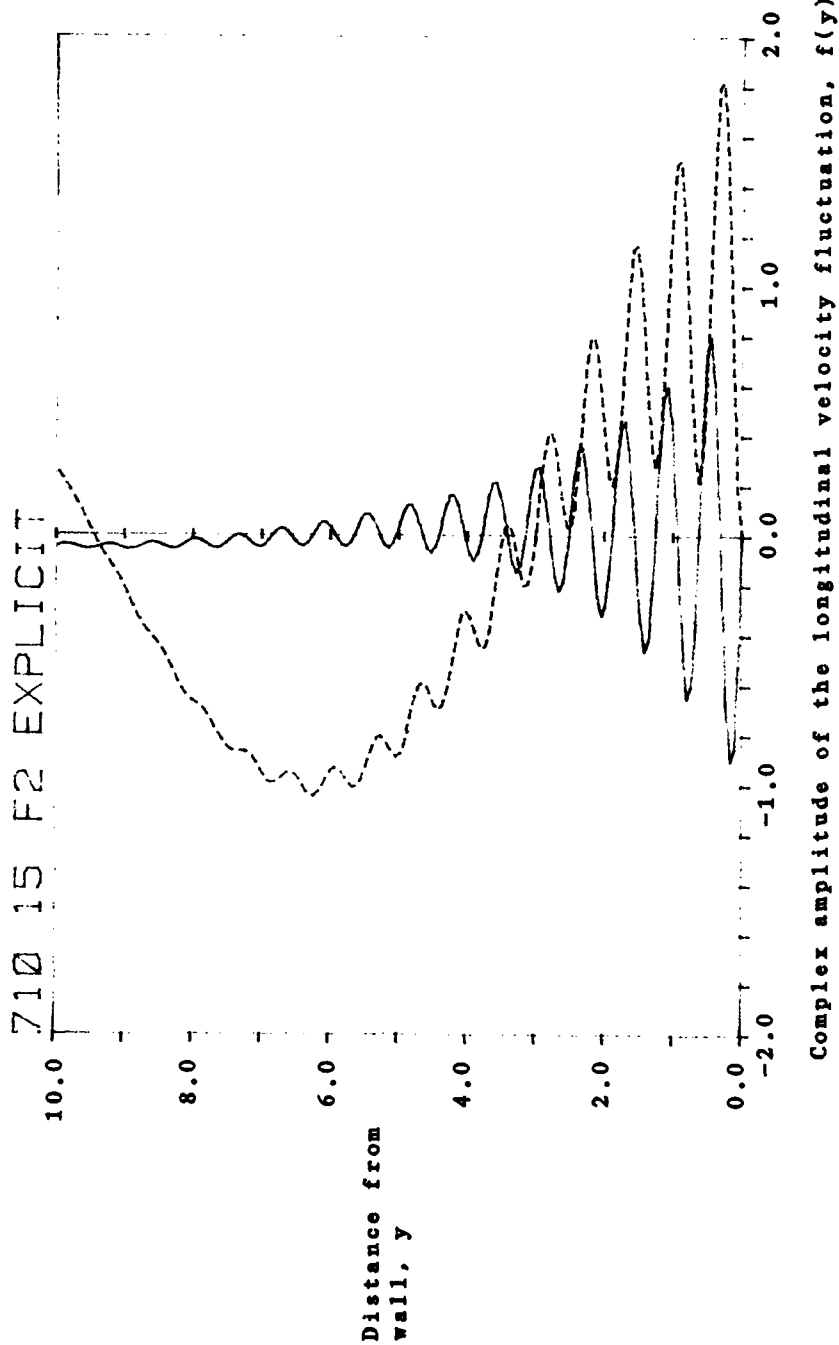


Figure 1.3 Explicit solution for the longitudinal velocity fluctuation for $\beta = \omega = 0.5$, $\gamma = 0$, $Re = 10$ and a uniform mean flow. The effect of Reynolds number on the high frequency oscillation can be seen by comparing this figure with Figure 1.8

$$Z(y) = -\frac{(a^2 + \beta^2)}{ia} \cos \beta y + \frac{m(a^2 + \beta^2)}{ia\beta} \sin \beta y \quad (\text{for } \gamma = 0) \quad (1.21b)$$

This amplitude is plotted in Figure 1.4. Note that there are no high frequency oscillations; the term $\exp(-my)$ is irrotational. Also note that there is no evidence of large amplitude spikes of vorticity at the wall associated with viscous sublayers. The sinusoidal oscillations are undamped and represent one part of the vortical freestream disturbances.

The fluctuating pressure

$$p = \pi(y) e^{iax - i\omega t} \quad (\text{for } \gamma = 0) \quad (1.22)$$

can be found from the x-momentum equation

$$u_t + u_x = -p_x + \frac{1}{R_0} (u_{xx} + u_{yy}) \quad (\text{for } \gamma = 0) \quad (1.23)$$

Substituting for u , then

$$\pi(y) = \left[\frac{\omega}{a} - 1 - \frac{a}{iR_0} \right] f(y) + \frac{1}{iaR_0} f_{yy} \quad (\text{for } \gamma = 0) \quad (1.24)$$

The pressure is plotted in Figure 1.5. The presence of the wall strongly influences the pressure through the term $\exp(-my)$.

The streamlines and iso-vorticity contours are plotted in Figures 1.6 and 1.7. The influence of the wall, through the high frequency term $\exp(iR_0 y)$ can be clearly seen in the streamline pattern. A more subtle influence of the boundary conditions at the wall is that they dictate the value of the constant D in eqn.(1.16a). This influence of the wall does not vanish far away from the wall. Only this effect on the phasing of the oscillation remains in the iso-vorticity contours of Figure 1.7.

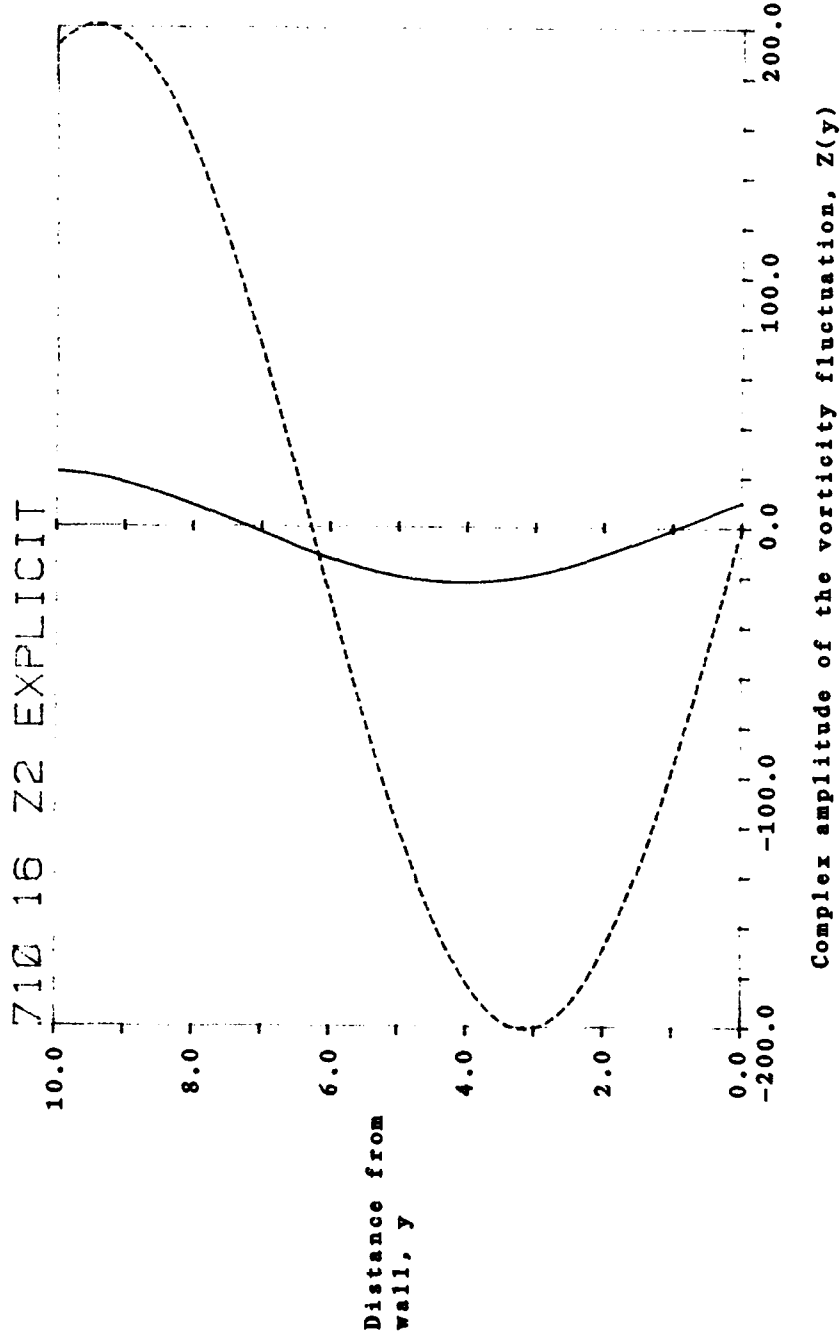


Figure 1.4 Explicit solution for the vorticity fluctuation for $\beta = \omega = 0.5$, $\gamma = 0$, $R_0 = 10$ and a uniform mean flow. The high frequency oscillations in Figures 1.2 and 1.3 do not appear here because the high-frequency oscillations are irrotational when the flow is uniform.

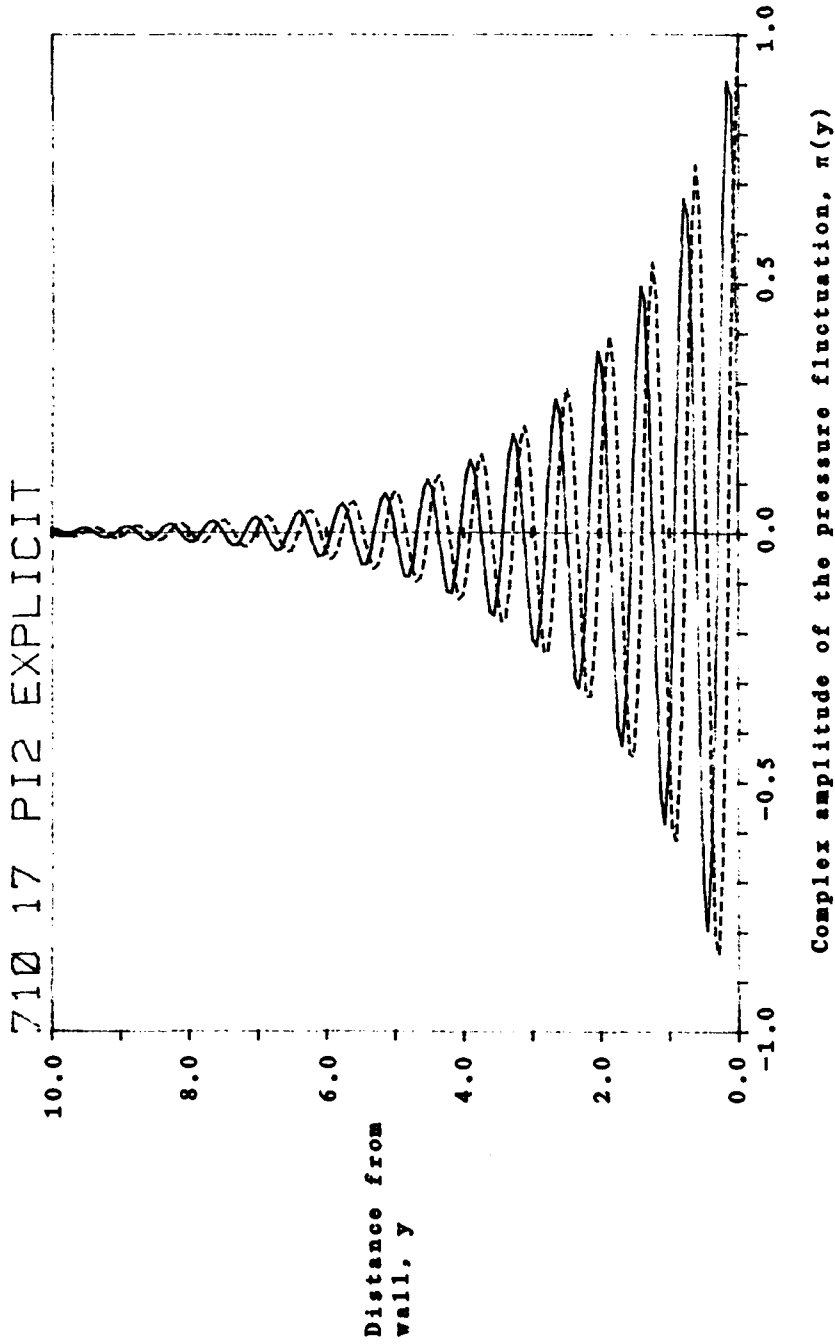


Figure 1.5 Explicit solution for the pressure fluctuation for $\beta = \omega = 0.5$, $\gamma = 0$, $R_0 = 10$ and a uniform mean flow.

710 01 STREAMLINES

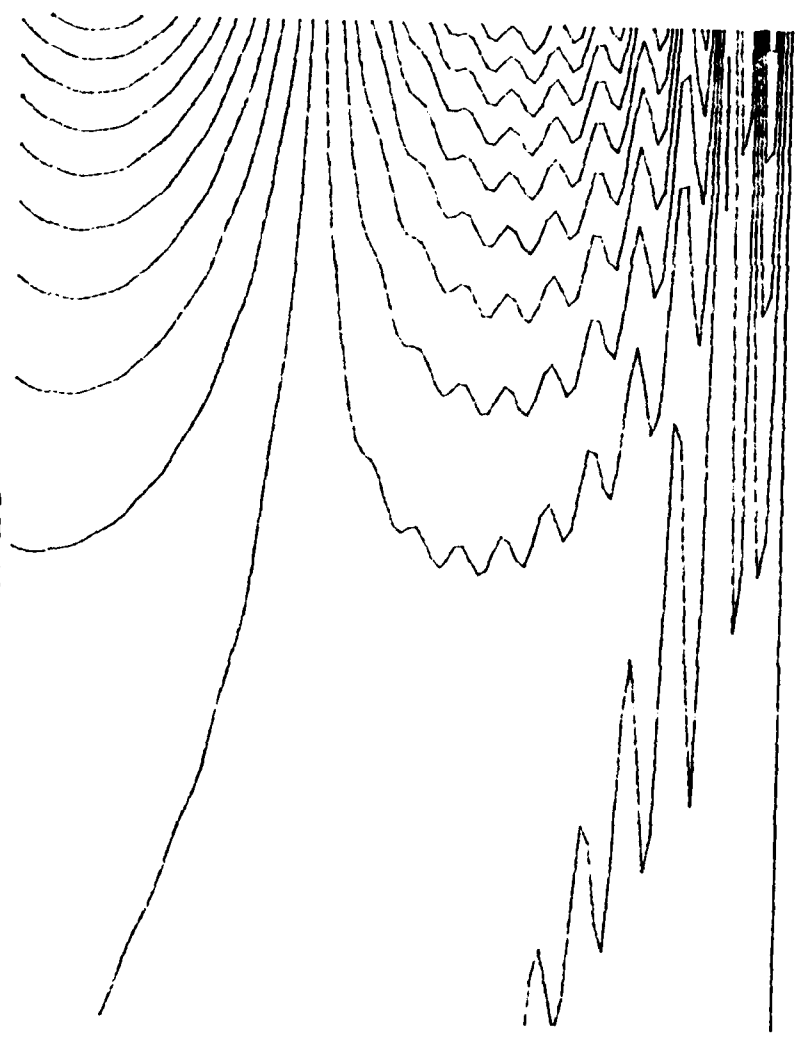


Figure 1.6 Streamlines of the fluctuating flow for $\beta = \omega = 0.5$, $\gamma = 0$, $R_6 = 10$ and a uniform mean flow. The x-coordinate is greatly stretched to show details. The y-scale is the same as for the other figures.

710 02 EQUI-VORTICITY CONTOURS

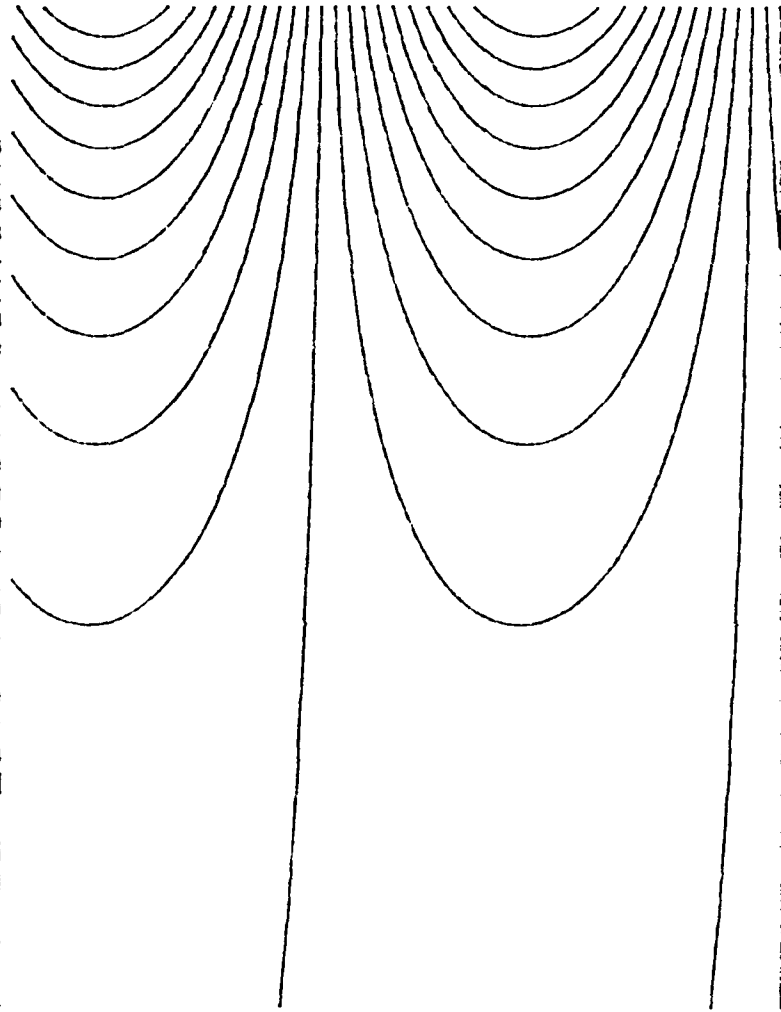


Figure 1.7 Equi-vorticity contours of the fluctuating flow for $\beta = \omega = 0.5$, $\gamma = 0$, $R_0 = 10$ and a uniform mean flow. The x-coordinate is greatly stretched to show details. The high-frequency waves of Figure 1.6 do not appear in the equi-vorticity contours when the flow is uniform.

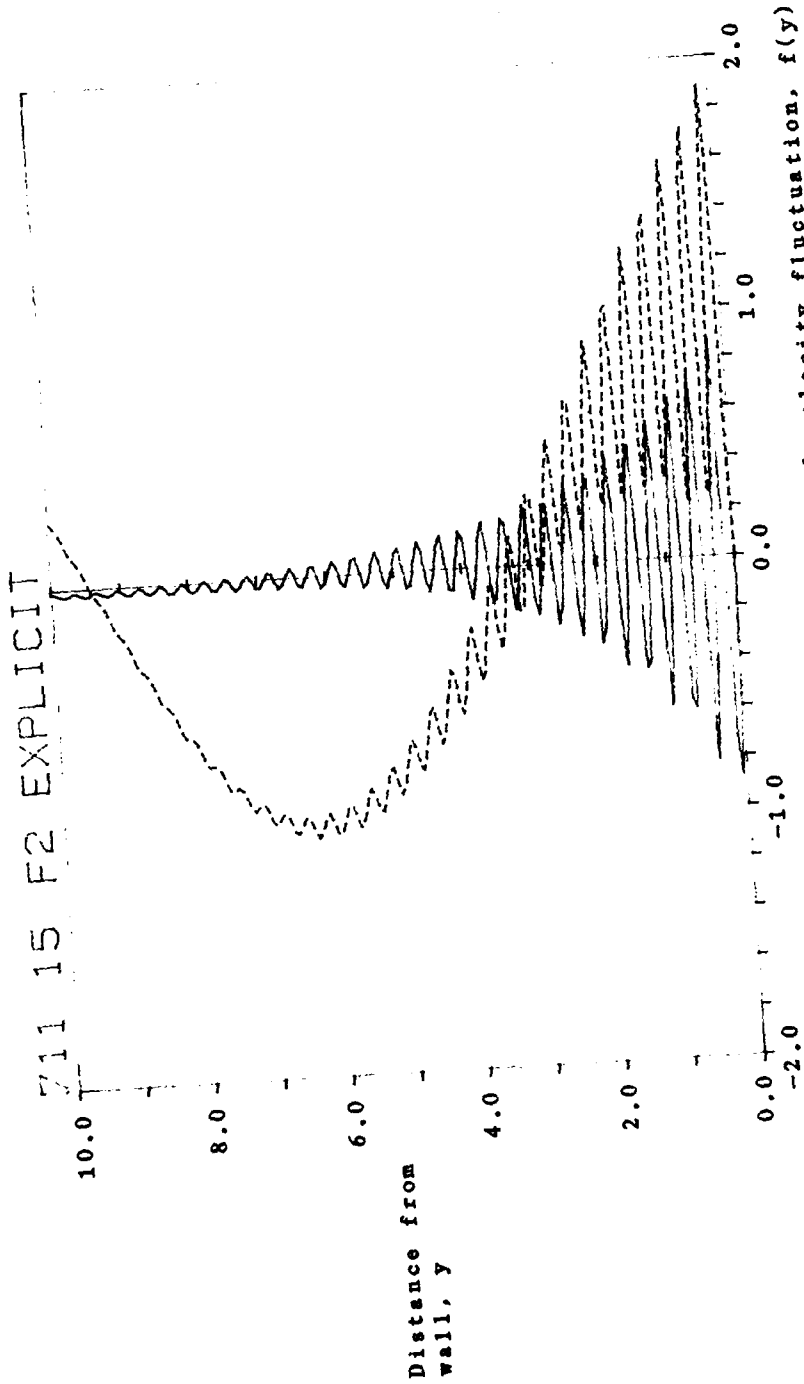


Figure 1.8 Explicit solution for the longitudinal velocity fluctuation for $\beta = \alpha = 0.5$, $\gamma = 0$, $R_0 = 20$ and a uniform mean flow. This figure can be compared with Figure 1.3 to see the effect of Reynolds number on the high frequency oscillation.

2. FORMULATION OF THE MATHEMATICAL SYSTEM FOR 3-D FLUCTUATIONS INTERACTING WITH BOUNDARY LAYERS

The linearized, parallel-flow, viscous momentum equations can be combined into the following equation in terms of the fluctuating velocity, $v(x,y,z,t)$, in the direction normal to the plate

$$\left\{ \frac{\partial}{\partial t} + \bar{U}(y) \frac{\partial}{\partial x} - \frac{1}{R_\delta} \nabla^2 \right\} \nabla^2 v - \bar{U}_{yy}(y) \frac{\partial v}{\partial x} = 0 \quad (2.1)$$

where the Laplacian is $\nabla^2 = \partial^2/\partial x^2 + \partial^2/\partial y^2 + \partial^2/\partial z^2$. The Reynolds number based upon the freestream velocity and characteristic thickness of the boundary layer is $R_\delta = \rho U_\infty \delta / \mu$. For Blasius boundary layers, the characteristic thickness is

$$\delta = (2\mu x / \rho U_\infty)^{1/2} \quad (2.2)$$

The lengths in eqn. 2.1 are nondimensionalized against δ and the time is nondimensionalized against δ/U_∞ . We now seek solutions of form

$$v(x,y,z,t) = \phi(y) \exp[i\alpha x + i\gamma z - i\omega t] \quad (2.3)$$

where the wavenumbers and the frequency are related by eqn. (1.11). The x -wavenumber is complex, while the z -wavenumber and frequency are real. Substituting eqn. (2.3) into (2.1), then after some rearrangement, the Orr-Sommerfeld equation results

$$\left\{ (\bar{U} - \frac{\omega}{\alpha}) (D^2 - \alpha^2 - \gamma^2) - \bar{U}_{yy} - \frac{1}{i\alpha R_\delta} (D^2 - \alpha^2 - \gamma^2)^2 \right\} \phi = 0 \quad (2.4)$$

where $D = d/dy$. This equation is subject to impermeability and no-slip at the wall and boundedness far away

$$\phi = D\phi = 0 \text{ at } y = 0 \text{ and } \phi \text{ is bounded as } y \rightarrow \infty \quad (2.5)$$

When $\bar{U} = 1$ outside the boundary layer, the system reduces to

$$\left[1 - \frac{\omega}{\alpha} - \frac{1}{i\alpha R_\delta} (D^2 - \alpha^2 - \gamma^2) \right] (D^2 - \alpha^2 - \gamma^2) \phi = 0 \quad (2.6)$$

Seeking solutions of form $\exp(m y)$, then the four solutions are

$$\exp(\pm i\beta y) \text{ or } \cos\beta y \text{ and } \sin\beta y \text{ (which oscillate neutrally)}$$

$$\text{and } \exp(\pm m y) \text{ (which oscillate and grow or decay)} \quad (2.7)$$

where m is the root with positive real part

$$n = (\alpha^2 + \gamma^2)^{1/2} \quad (2.8)$$

Hence the solution outside of the boundary layer is

$$\phi(y) = Ae^{-ny} + Be^{+ny} + C\cos\beta y + D\sin\beta y \quad (\text{for } y > y_e) \quad (2.9)$$

where $B = 0$ in the present problem and we normalize by setting $C = 1$. We require that the exterior solution and the first three derivatives agree with the interior solution and the corresponding derivatives at the "edge" of the boundary layer, $y=y_e$

$$D^n\phi(y_e^-) = D^n\phi(y_e^+) \quad \text{for } n = 0,1,2,3 \quad (2.10)$$

With the normal velocity found as a solution of the Orr-Sommerfeld equation, then the longitudinal velocity is found from the continuity equation. The vorticity is calculated from the derivatives of the velocities, and the pressure is found from the x-momentum equation. rms quantities and other correlations such as the Reynolds stress and energy production are also found.

Our objective now is to solve the mathematical system composed of the Orr-Sommerfeld equation (2.6a,b), the two wall conditions (2.8), and the four conditions at the boundary layer edge (2.10).

3. NUMERICAL SOLUTIONS FOR WAVES TRAVELING UPSTREAM IN BOUNDARY LAYERS

3.1 SUMMARY OF THE NUMERICAL TECHNIQUES

The numerical techniques for calculating both the mean flow and the unsteady flow are the same as used in Refs. 13 and 14. The numerical techniques are summarized in this section.

To obtain the coefficients $\bar{U}(y)$ and $\bar{U}_{yy}(y)$ of the mean flow, numerical solutions of the Falkner-Skan equation are obtained by the method of Nachtsheim and Swigert (Ref. 15). The equation is solved by shooting from the wall outward, using 4th-order Runge-Kutta integration in double-precision arithmetic. The exterior boundary condition, $F = 1$ as $\eta \rightarrow \infty$, is not specified at the boundary layer edge, $y = y_e$, but rather the error is minimized in a least square sense.

The Orr-Sommerfeld system of equations (2.6b, 2.8, 2.13, 2.14) is solved by an expansion in Chebyshev polynomials

$$\phi(\hat{\eta}) = \sum_{m=0}^{N-1} a_m T_m(\hat{\eta}) \quad (3.1)$$

with polynomials defined as

$$T_m(\hat{\eta}) = \cos[m(\arccos \hat{\eta})] \quad (3.2)$$

and where the variable $\hat{\eta}$ is related to the dimensionless y by the linear transformation

$$\hat{\eta} = \frac{2y}{y_e} - 1 \quad (3.3)$$

A set of linear, algebraic equations results from the Orr-Sommerfeld equation, the two wall boundary conditions, and the four matching conditions at the boundary layer edge. The matrix of coefficients for this system is reduced by Gauss-Jordan elimination with maximum pivoting by column and rows. With the coefficients known, the expansion 3.1 is carried out for $\phi(y)$, and identities used to obtain the y -derivatives of $\phi(y)$. With ϕ and its derivatives known, the longitudinal velocity, vorticity, and vorticity production are calculated. From the x -momentum equation, the pressure fluctuations are found, and then the correlations are calculated for the rms quantities. The streamlines and iso-vorticity contours are also drawn.

The numerical checks include numerical experiments to determine the effects of number of terms in the expansion, precision of arithmetic for the matrix reduction, and influence of the y -value where the edge boundary conditions are imposed. Comparisons are made between analytical and numerical solutions for a uniform mean flow. The same computer program used to obtain solutions for the traveling waves, except with different patching conditions at the boundary layer edge, was also used to recover the Tollmien-Schlichting waves, the two standing waves, decaying vortical fluctuations in the

freestream, and decaying longitudinal vortices.

3.2 NUMERICAL RESULTS FOR UPSTREAM TRAVELING WAVES IN A BLASIUS BOUNDARY LAYER

The velocity profile and derivatives for the Blasius boundary layer are plotted in Figure 3.1 with the same y-scale as the other figures.

To aid in the interpretation of these calculations, since

$$\begin{aligned} v &= [\theta_r(y) + i\theta_i(y)]e^{i\alpha_r x - i\omega t} e^{-\alpha_i x} \\ &= \theta_r \cos(\alpha_r x - \omega t) e^{-\alpha_i x} - \theta_i \sin(\alpha_r x - \omega t) e^{-\alpha_i x} \end{aligned} \quad (3.4)$$

then for

$$\begin{aligned} \alpha_r x - \omega t = 0, & \quad v = \theta_r(y) e^{-\alpha_i x} \\ \alpha_r x - \omega t = \pi/2, & \quad v = -\theta_i(y) e^{-\alpha_i x} \\ \alpha_r x - \omega t = \pi, & \quad v = -\theta_r(y) e^{-\alpha_i x} \\ \alpha_r x - \omega t = 3\pi/2, & \quad v = \theta_i(y) e^{-\alpha_i x} \end{aligned} \quad (3.5a-d)$$

The vertical lines $\alpha_r x - \omega t = 0, \pi/2, \pi,$ and $3\pi/2$ travel to the left at speed $c_{ep} = \omega/\alpha_r$ (slightly less than -1). Hence the real and imaginary parts of the complex amplitude (when multiplied by the factor $\exp(-\alpha_i x)$) are the velocity profiles along those vertical lines $\alpha_r x - \omega t = 0$ and $3\pi/2$ respectively. With a reversal of sign, they are the velocity profiles along the lines $\alpha_r x - \omega t = \pi/2$ and π . Analogous interpretations also apply for the other complex amplitudes.

Figures 3.2 through 3.15 are plots for a wave with y-wavenumber and frequency, $\beta = \omega = 0.5$, and Reynolds number $R_\delta = 10$. These calculations are for 2-D fluctuations, although the computer program for $\theta(y)$ is applicable for 3-D fluctuations.

In Figure 3.2 for the normal velocity, note that the impermeability condition is satisfied at the wall. Also note the dual oscillatory behavior of the solution. Far from the boundary

$$\theta(y) = \cos\beta y + D\sin\beta y \quad (3.6)$$

This figure (with a Blasius layer) can be compared with Figure 1.2 (with a uniform mean flow). Note the substantial influence of the boundary layer on both the magnitude of the high-frequency oscillations and the phasing of the low-frequency oscillations ($\sin\beta y$ and $\cos\beta y$) which survive into the freestream.

Figure 3.3 is a plot of the rms normal velocity fluctuation which shows that impermeability is satisfied and illustrates the slow dampening of the high-frequency oscillation in the y-direction.

In Figure 3.4 for the longitudinal velocity, note that the no-slip condition is satisfied and again note the general oscillatory behavior of the solution. This figure (with a Blasius layer) can be compared with Figure 1.3

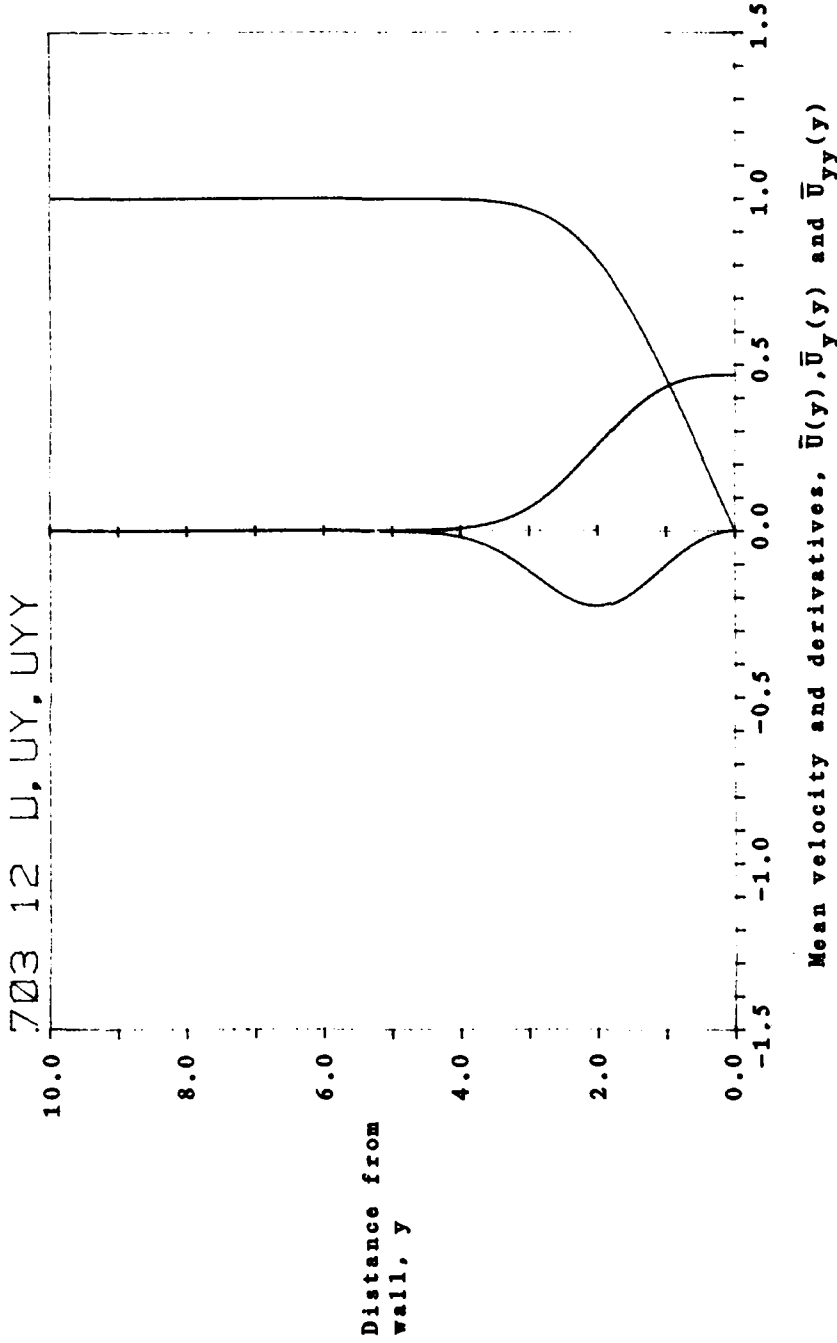


Figure 3.1 The mean velocity profile and derivatives for a Blasius boundary layer.

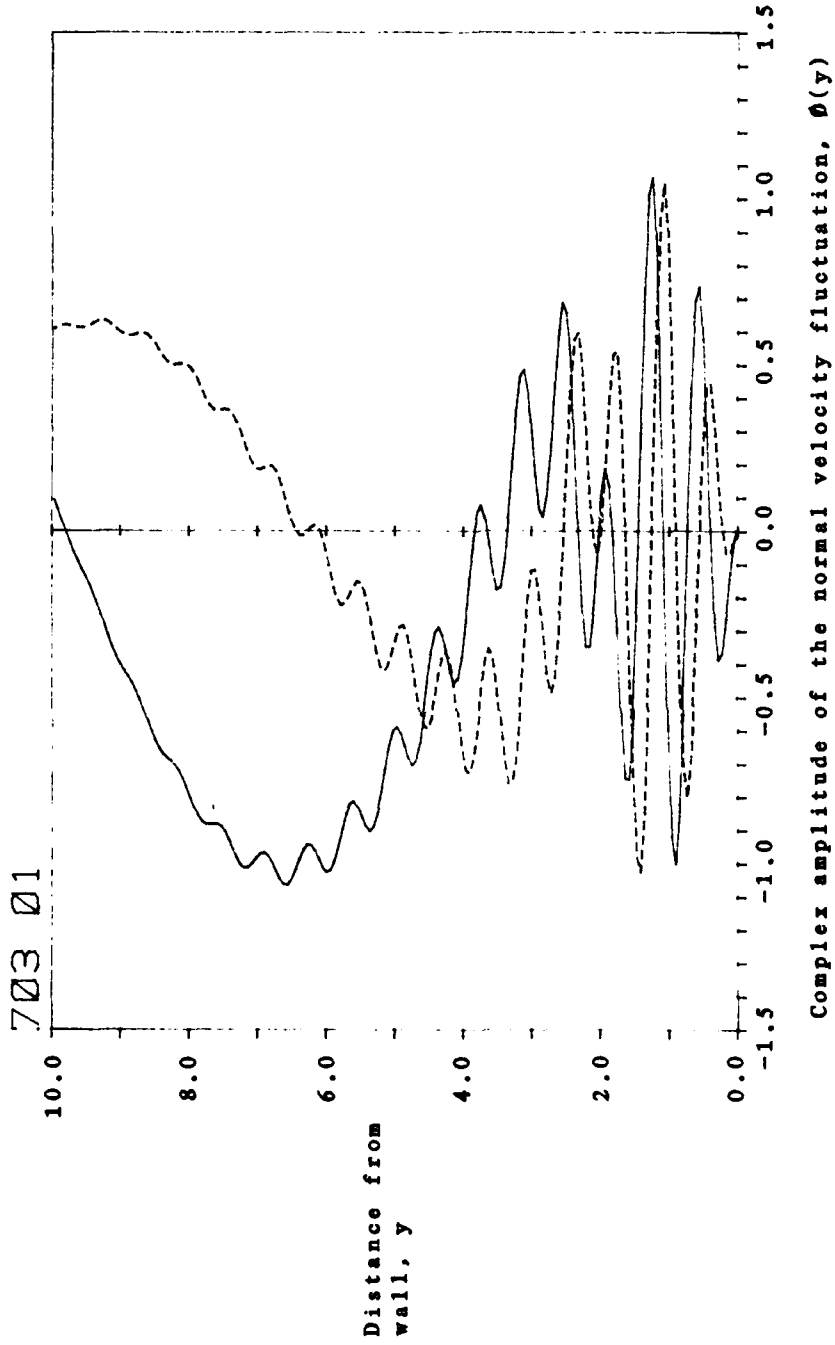


Figure 3.2 Calculation of the normal velocity fluctuation for $\beta = \omega = 0.5$, $\gamma = 0$, $R_0 = 10$ and a Blasius boundary layer. This figure (for a Blasius layer) can be compared with Figure 1.2 (for a uniform mean flow).

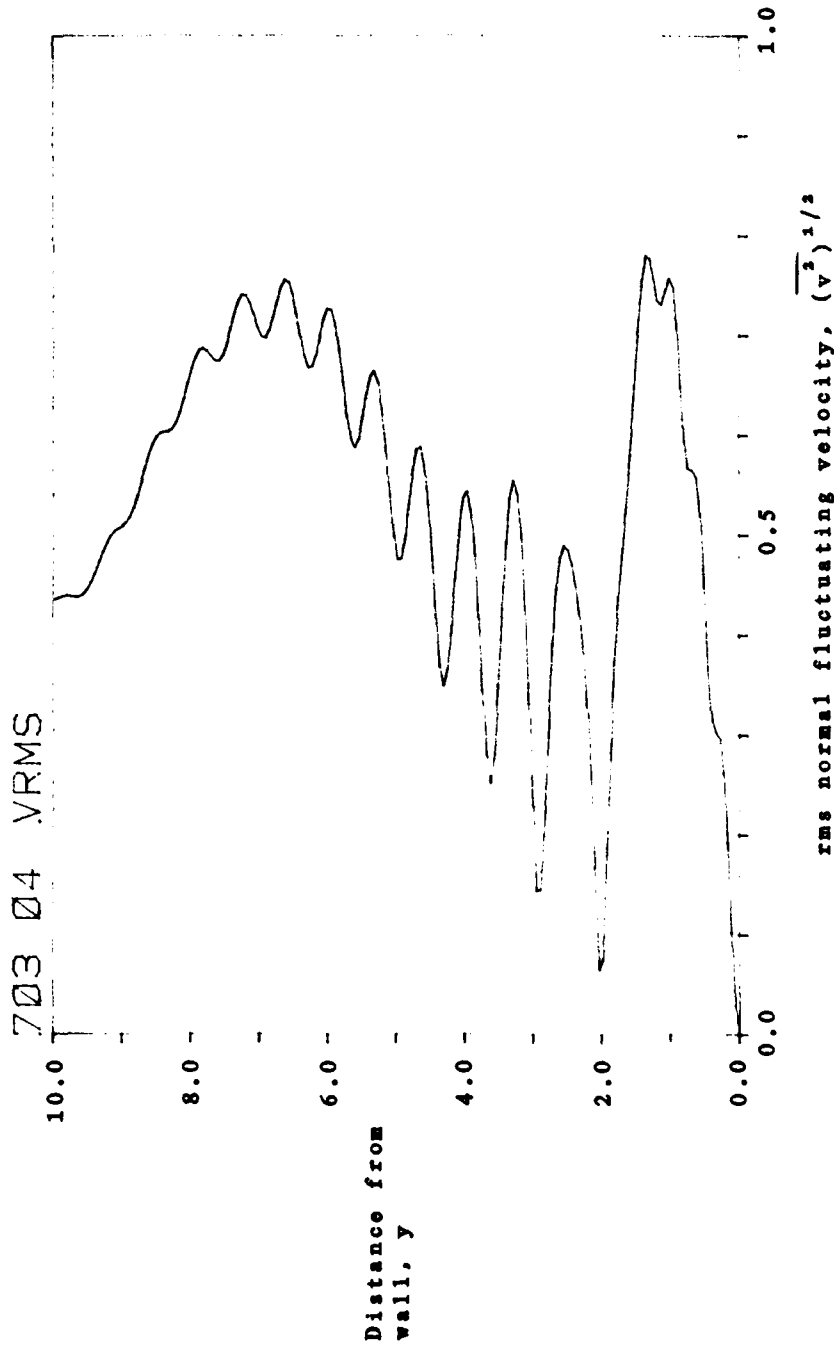


Figure 3.3 Calculation of the rms normal velocity fluctuation for $\beta = \omega = 0.5$, $\gamma = 0$, $R_0 = 10$ and a Blasius boundary layer.

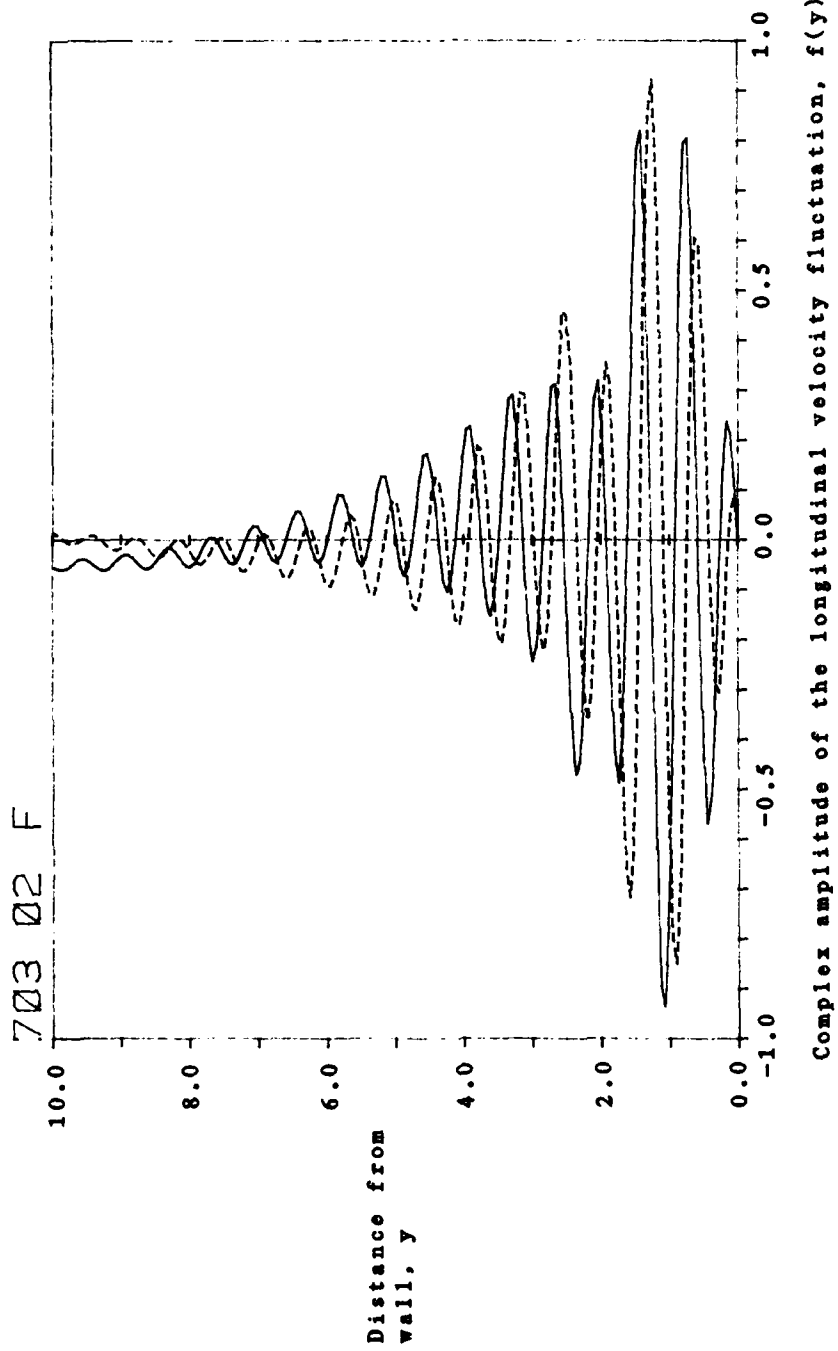


Figure 3.4 Calculation of the longitudinal velocity fluctuation for $\beta = \omega = 0.5$, $\gamma = 0$, $R_0 = 10$ and a Blasius boundary layer. This figure (for a Blasius layer) can be compared with Figure 1.3 (for a uniform mean flow).

(for a uniform mean flow). While both figures illustrate the dual oscillatory behavior, the details of the flows are quite different. The y -wavenumber, frequency, and Reynolds number are the same for both figures.

Figure 3.5 is the rms version of the previous figure which illustrates the slow dampening of the high-frequency oscillation.

The streamlines for the fluctuating flow at time zero are plotted in Figure 3.6. Again note the dual oscillatory patterns in the y -direction and the effects of the exponential growth in the streamwise direction, behaving approximately as $\exp(+R_\delta x)$. When comparing Figure 3.6 (with a Blasius layer) and Figure 1.6 (with a uniform mean flow), note the much stronger high frequency oscillations in Figure 3.6.

The fluctuating vorticity, $\xi = v_y - u_x$, is plotted in Figure 3.7; the rms vorticity is plotted in Figure 3.8. In contrast to Figure 1.4 where no high frequency oscillations are present, Figures 3.7 and 3.8 clearly show that such oscillations arise when the boundary layer is present.

The source of the high frequency rotational fluctuations when the boundary layer is present is shown in Figure 3.9, which is a plot of the vorticity production term in the equation describing the evolution of vortical fluctuations in the boundary layer

$$\xi_t + \bar{u}\xi_x + v\bar{\xi}_y = s(\xi_{xx} + \xi_{yy}) \quad (3.7)$$

where $v\bar{\xi}_y = -\partial(y)\bar{u}_{yy}(y)\exp(iax-i\omega t)$

This term is analogous to the term describing the production of disturbance energy in shear layers, $-uvd\bar{u}/dy$. The term $-\partial\bar{u}_{yy}$ is plotted as Figure 3.9 which shows that the high-frequency velocity produces high frequency vorticity. The vorticity which has been produced appears in Figures 3.7 and 3.8 as the high frequency vortical fluctuations near the wall. This production vanishes at the wall (since $v=0$ there) and in the freestream (since $\bar{u}_{yy}=0$ outside of the boundary layer).

The iso-vorticity contours are plotted in Figure 3.10. This pattern is substantially simpler than the streamline pattern of Figure 3.6, but contains the high-frequency oscillation which Figure 1.7 does not have when the mean flow is uniform.

The complex amplitudes and the rms amplitude of the fluctuating pressure are plotted in Figures 3.11 and 3.12. Much of the high-frequency characteristics of the instantaneous pressure is lost by the rms version, at least for this particular case. Note that the pressure is not constant across the boundary layer.

The Reynolds stress, $-\bar{uv}$, and the kinetic energy production, $-\bar{uv}d\bar{u}/dy$, are plotted in Figures 3.13 and 3.14. The Reynolds stress again reflects the slowly decaying, high-frequency oscillation. The energy production is confined to the boundary layer. It vanishes at the wall where $v = 0$ and in

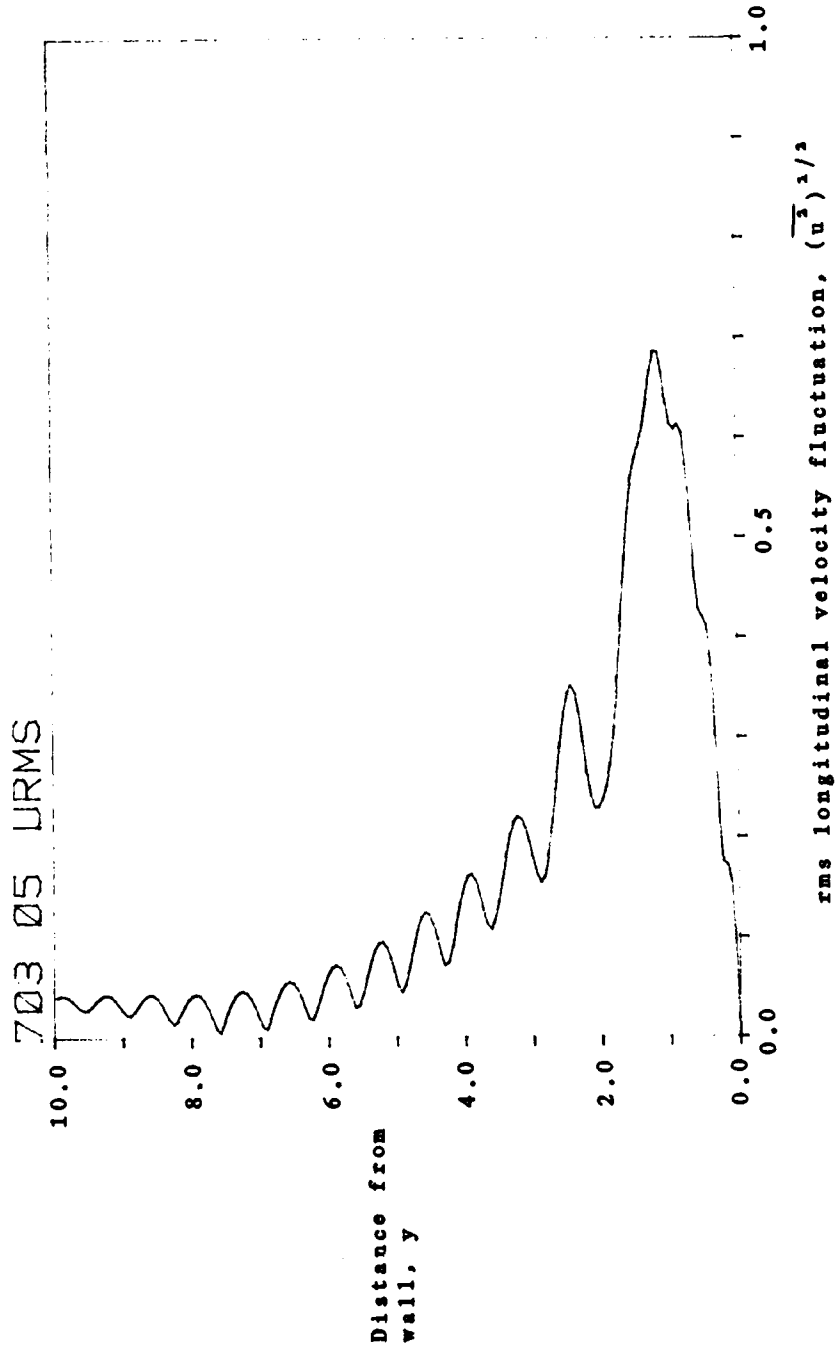


Figure 3.5 Calculation of the rms longitudinal velocity fluctuation for $\beta = \omega = 0.5$, $\gamma = 0$, $R_\delta = 10$ and a Blasius boundary layer.

703 01 STREAMLINES

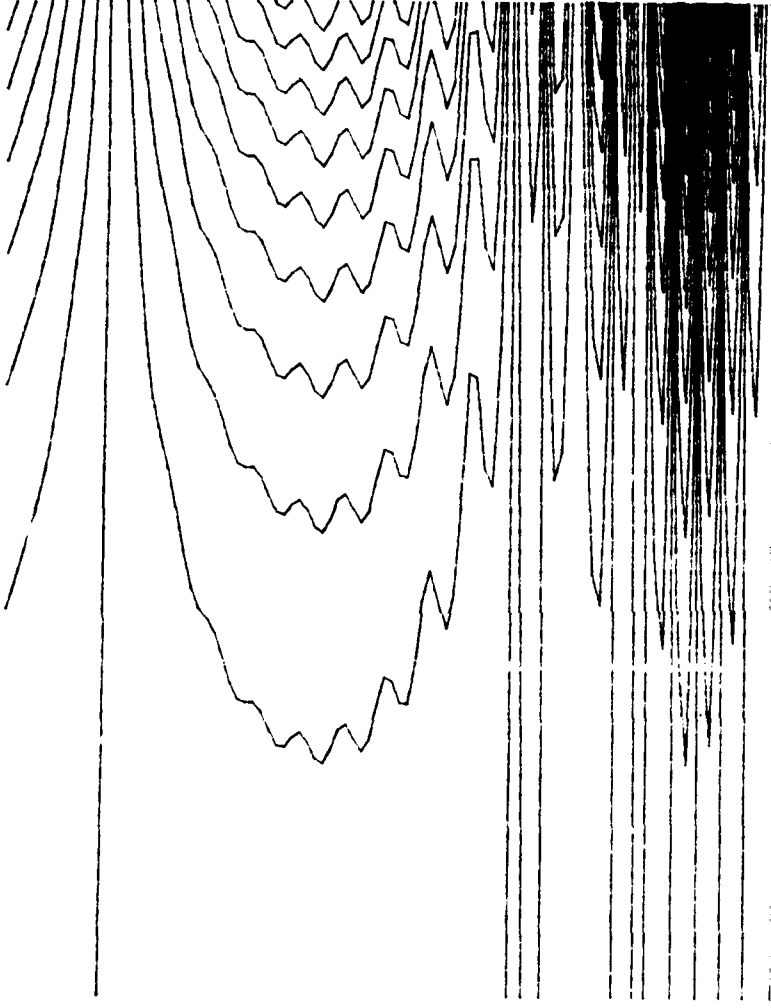


Figure 3.6 Streamlines of the fluctuating flow for $\beta = \omega = 0.5$, $\gamma = 0$, $R_0 = 10$ and a Blasius boundary layer. The x-coordinate is greatly stretched to show details. The grid is $50x$ by $100y$.

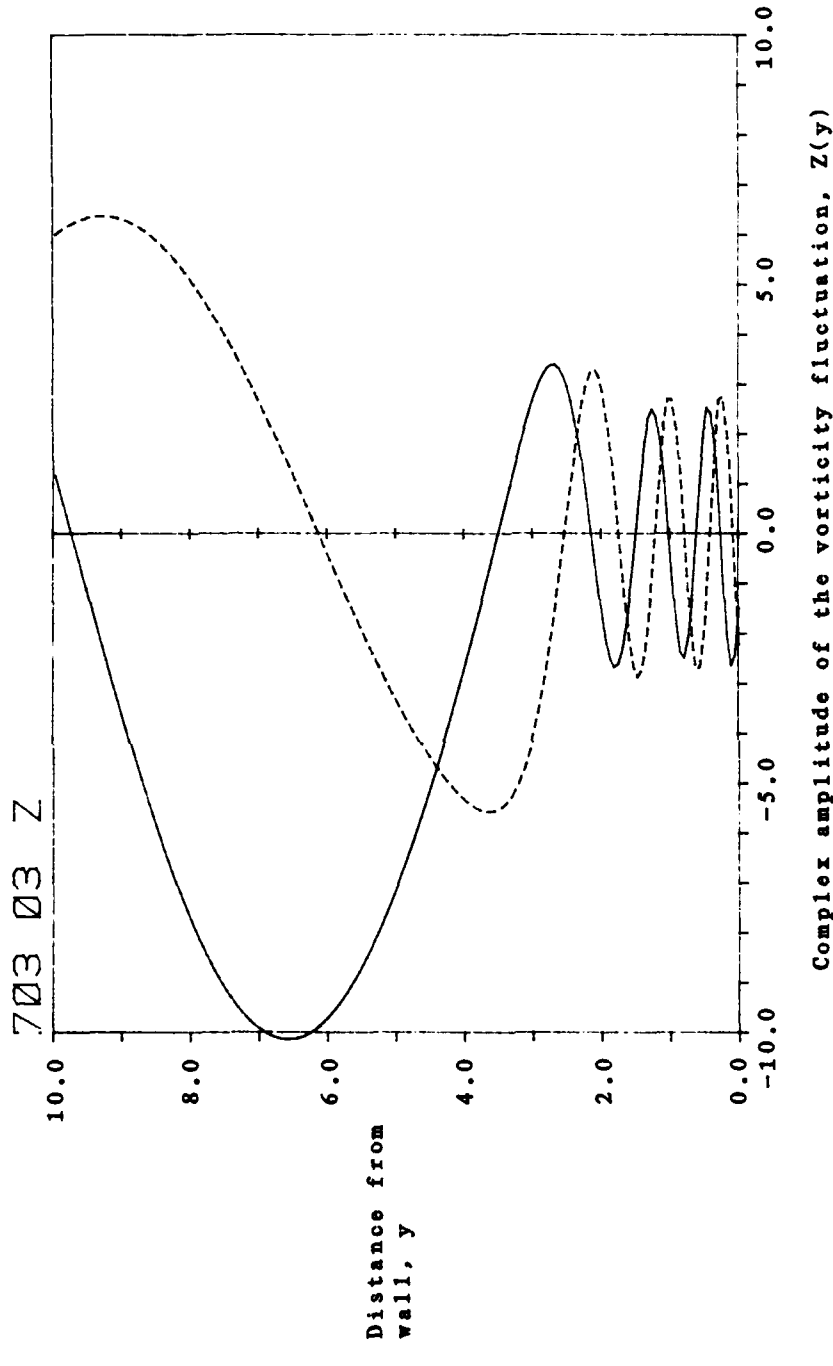


Figure 3.7 Calculation of the vorticity fluctuation for $\beta = \omega = 0.5$, $\gamma = 0$, $R_0 = 10$ and a Blasius boundary layer. This figure (for a Blasius layer) can be compared with Figure 1.4 (for a uniform mean flow). Note the appearance of high frequency rotational oscillations when the boundary layer is present.

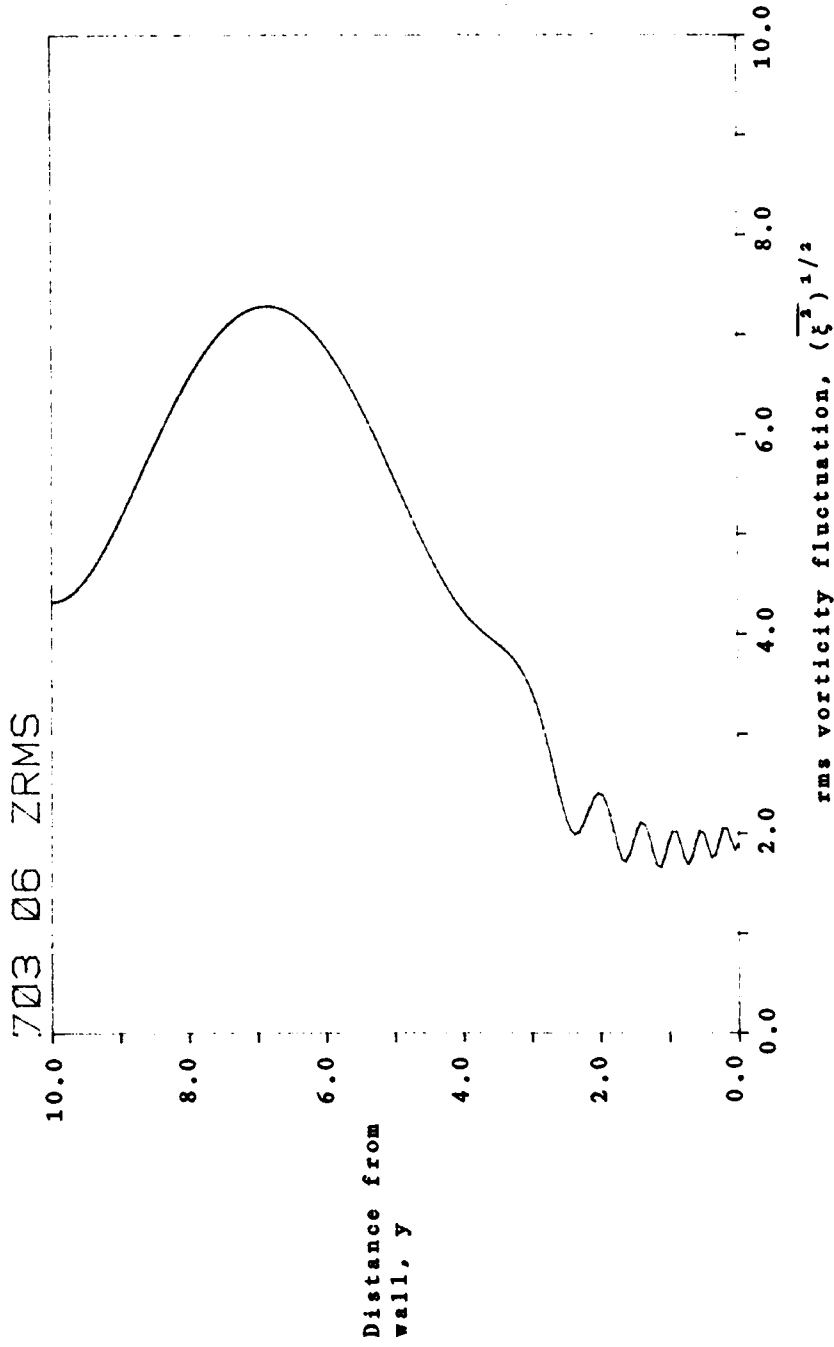


Figure 3.8 Calculation of the rms vorticity fluctuation for $\beta = \omega = 0.5$, $\gamma = 0$, $R_\xi = 10$ and a Blasius boundary layer.

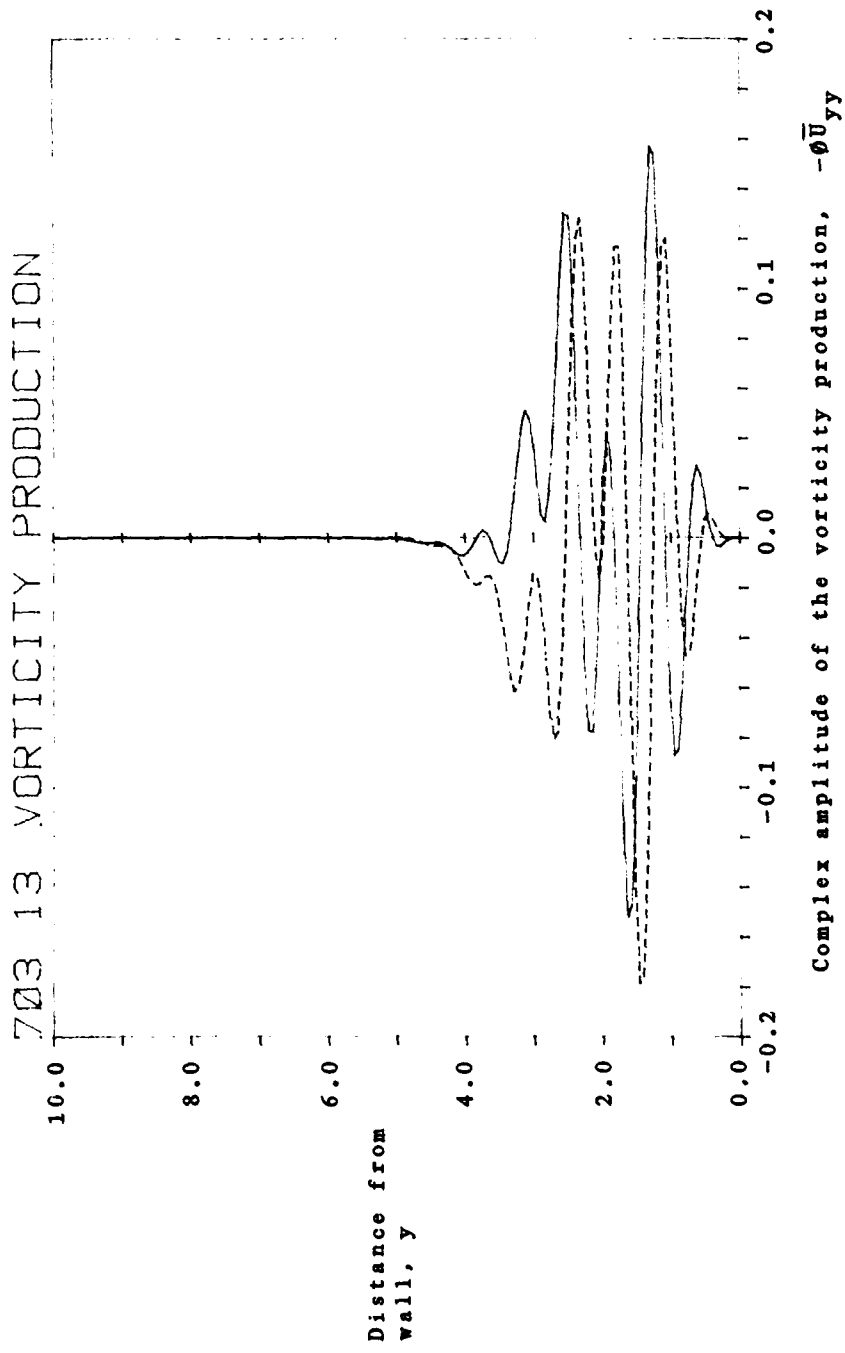


Figure 3.9 Calculation of the production of fluctuating vorticity for $\beta = \omega = 0.5$, $\gamma = 0$, $R_0 = 10$ and a Blasius boundary layer. This term vanishes for a uniform mean flow.

703 02 EQUI-VORTICITY CONTOURS

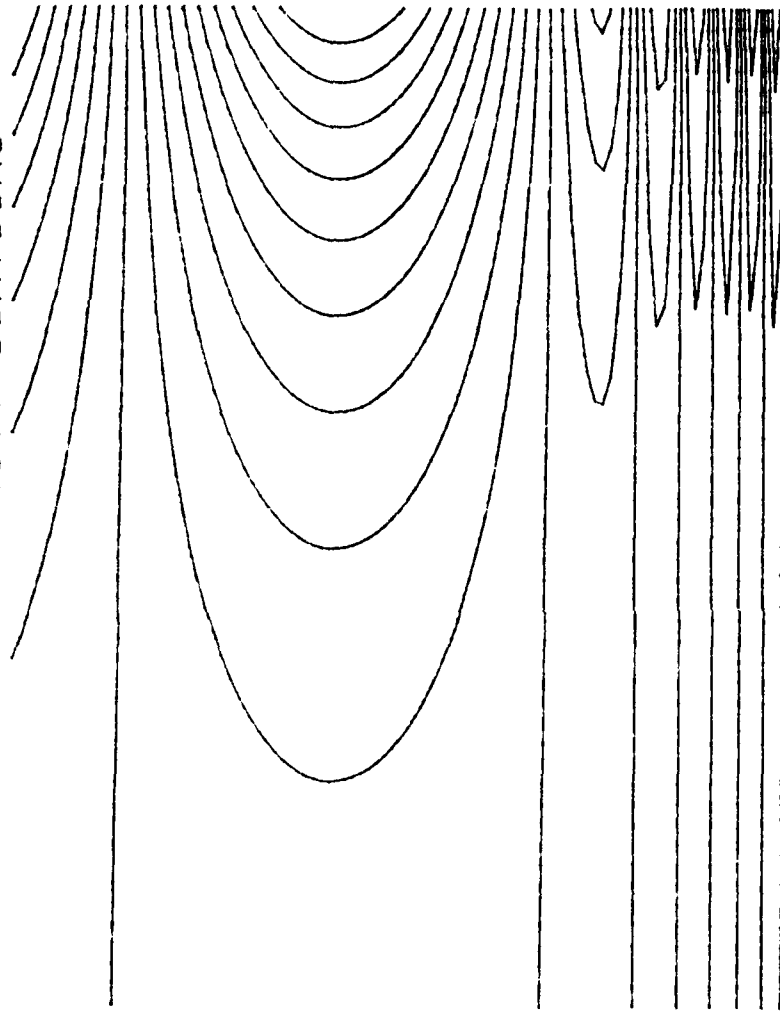


Figure 3.10 Contours of equi-vorticity for $\beta = \omega = 0.5$, $\gamma = 0$, $R_0 = 10$ and a Blasius boundary layer. This figure with a Blasius layer can be compared with Figure 1.7 with a uniform mean flow.

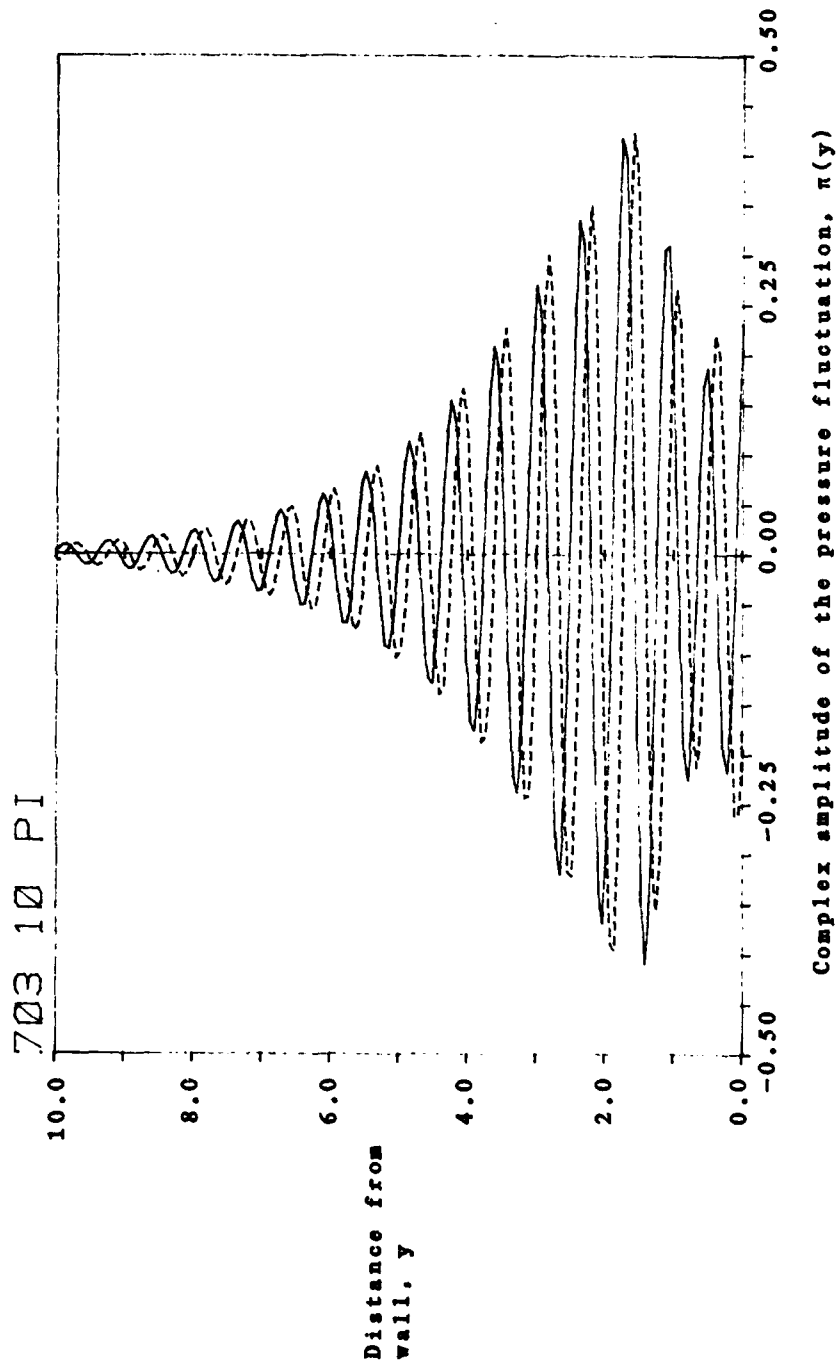


Figure 3.11 Calculation of the fluctuating pressure for $\beta = \omega = 0.5$, $\gamma = 0$, $R_0 = 10$ and a Blasius boundary layer. This figure (for a Blasius layer) can be compared with Figure 1.5 (for a uniform mean flow).

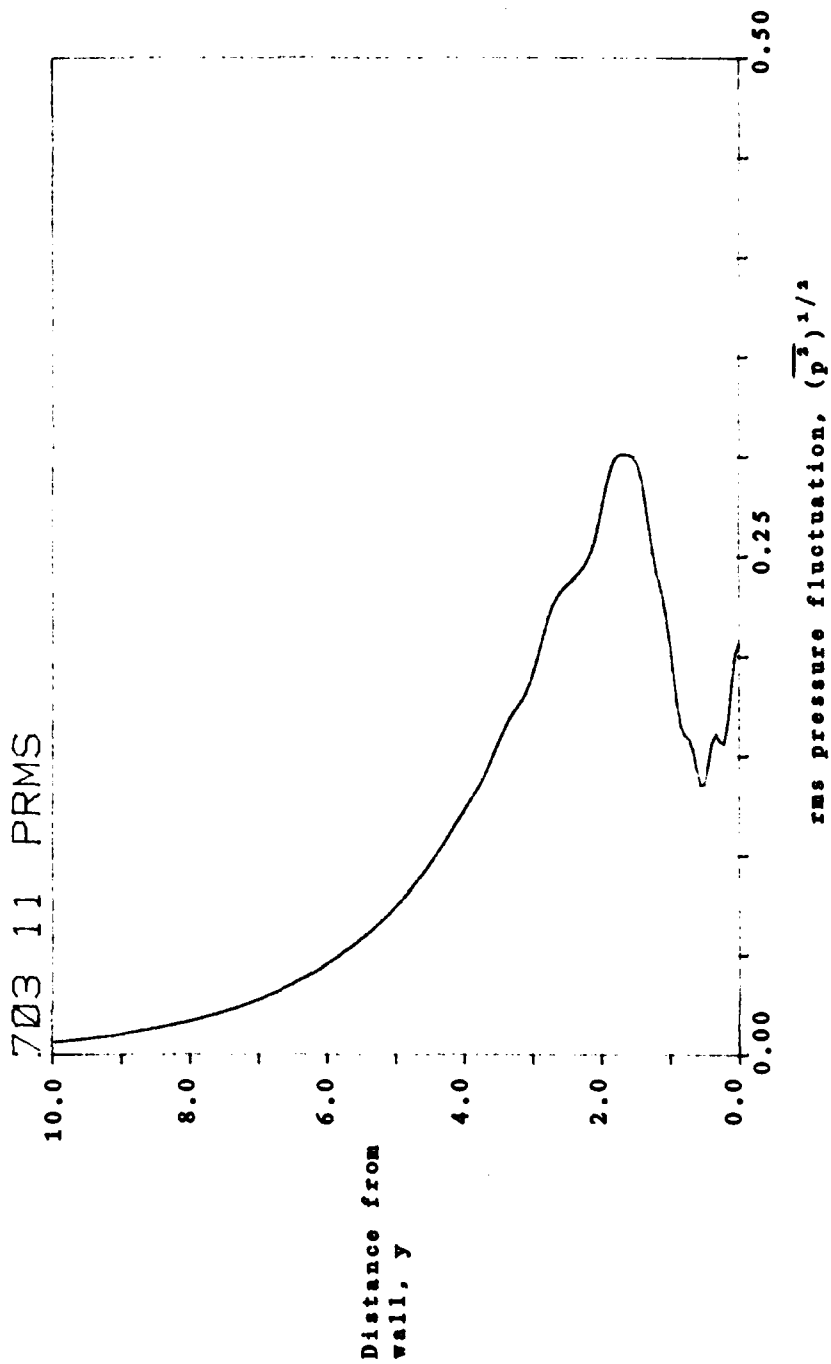


Figure 3.12 Calculation of the rms fluctuating pressure for $\beta = \omega = 0.5$, $\gamma = 0$, $R_0 = 10$ and a Blasius boundary layer.

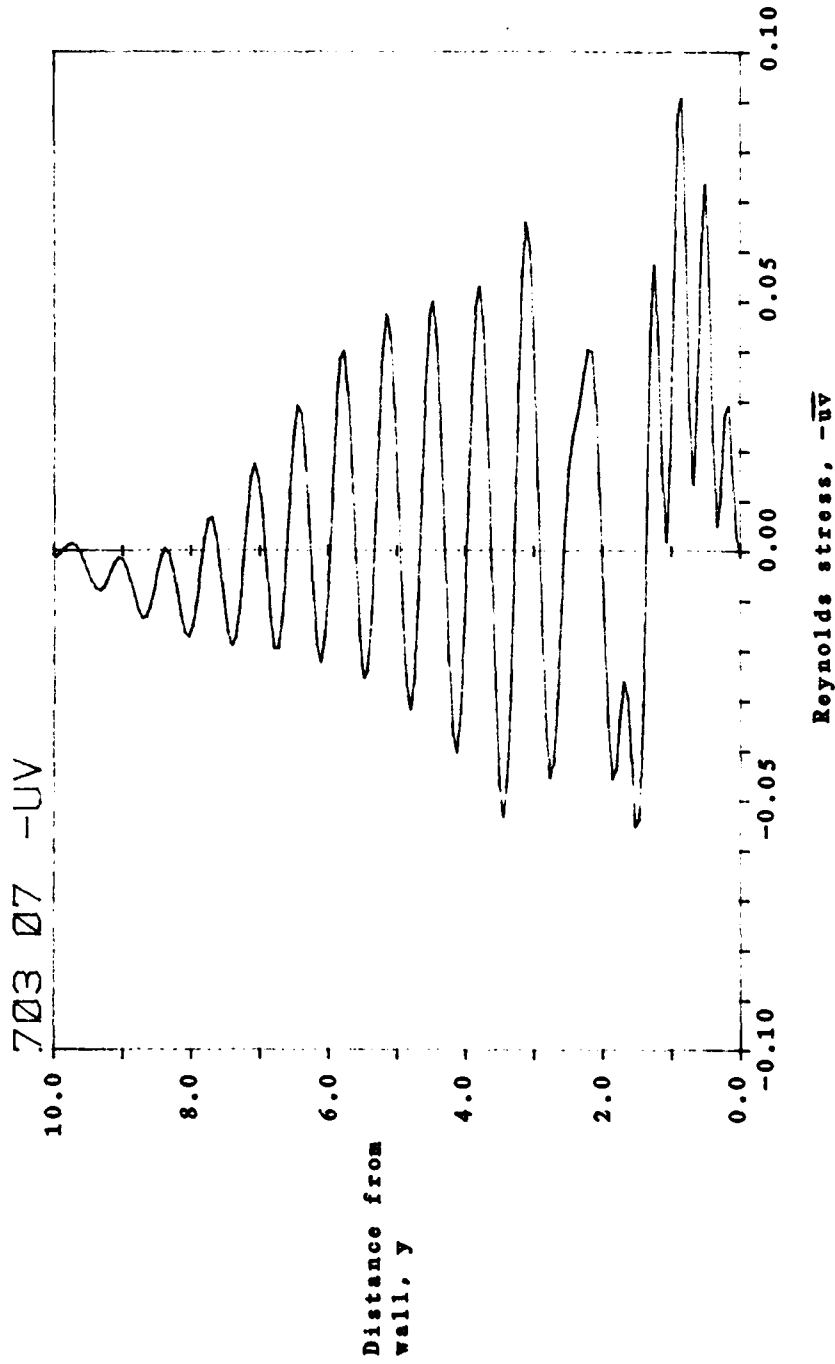


Figure 3.13 Calculation of Reynolds stress for $\beta = \omega = 0.5$, $\gamma = 0$, $R_0 = 10$ and a Blasius boundary layer.

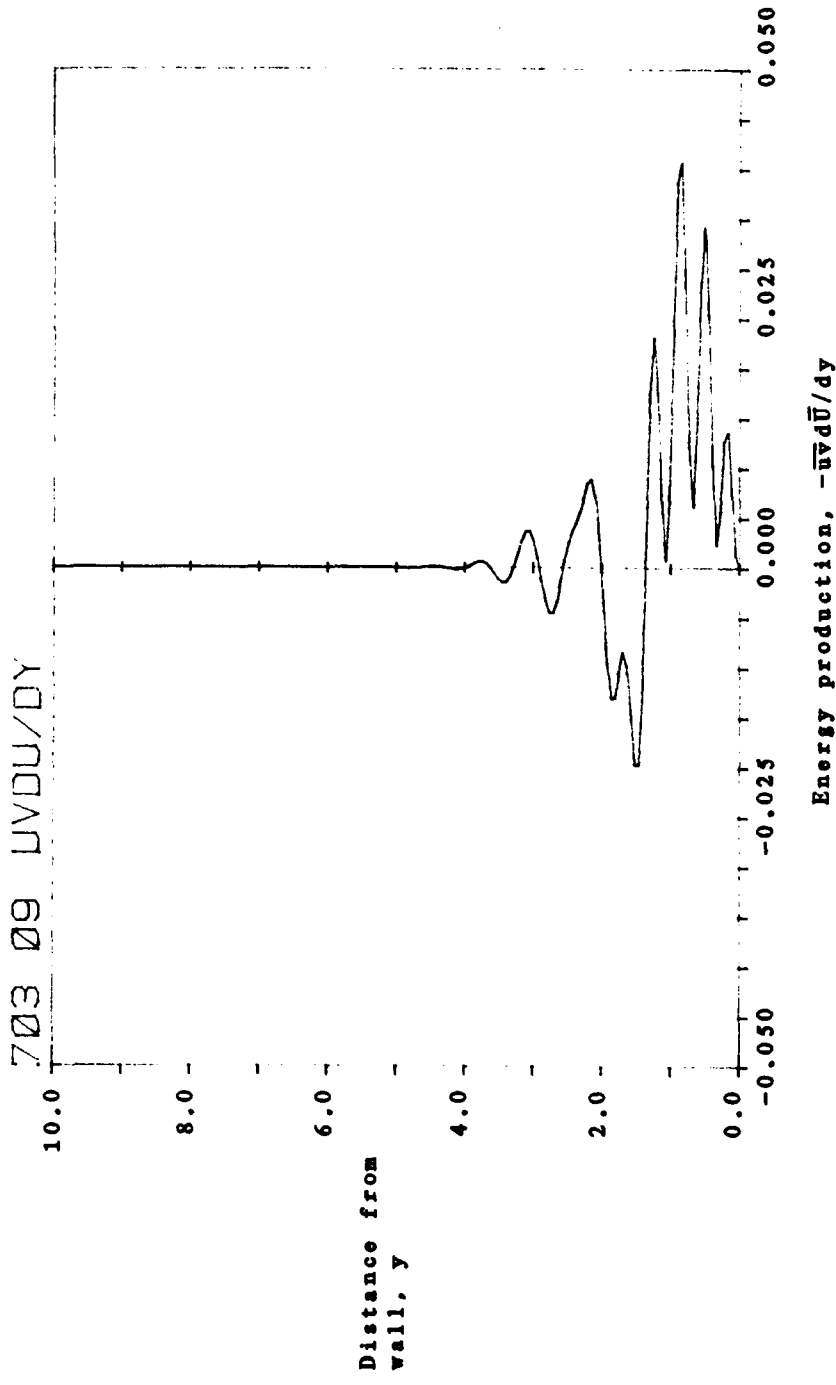


Figure 3.14 Calculation of the energy production for $\beta = \omega = 0.5$, $\gamma = 0$, $R_0 = 10$ and a Blasius boundary layer.

the freestream where $\bar{U}_y = 0$.

The averaged kinetic energy $(\bar{u}^2 + \bar{v}^2)/2$ of the unsteady flow is plotted in Figure 3.15, which illustrates that a region exists in the boundary layer where the kinetic energy is larger than in the freestream. This region roughly corresponds to the region where the energy production is positive in Figure 3.14.

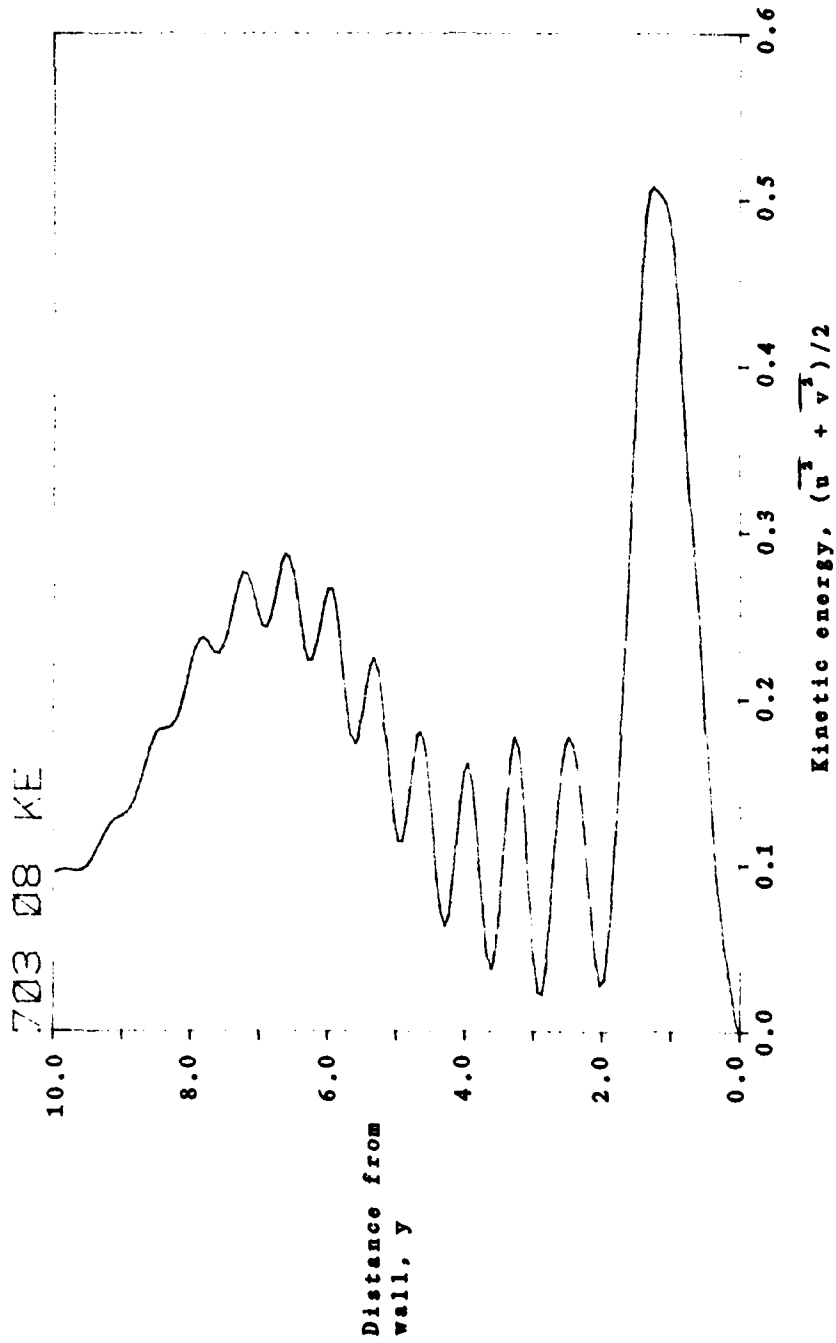


Figure 3.15 Calculation of the disturbance kinetic energy for $\beta = \omega = 0.5$, $\gamma = 0$, $R_\delta = 10$ and a Blasius boundary layer.

4. SUMMARY, DISCUSSION AND CONCLUSIONS

4.1 INTRODUCTORY COMMENTS

This report describes a fluctuation which propagates upstream in a boundary layer. This fluctuation diffuses in the upstream direction, against the mean flow, and dampens very rapidly in the upstream direction. The propagation speed is always more negative than $-U_{\infty}$ (i.e. the absolute value of the speed is always greater than U_{∞} and is directed upstream). As the Reynolds number increases, the speed approaches $-U_{\infty}$ as the Reynolds number becomes infinite.

These fluctuations oscillate sinusoidally in time. Far from the boundary layer, they oscillate sinusoidally in the y-direction.

Evidence of the existence of these waves is based on numerical solutions of the Orr-Sommerfeld equation, analytical solutions of simplified forms of the Orr-Sommerfeld equation, and an asymptotic solution of the Orr-Sommerfeld equation. The asymptotic solution is not summarized in this report, but a similar solution was used by Shunichi Tsuge' (Ref. 16) for the Tollmien-Schlichting wave. The use of that asymptotic solution in the spatial initial-value problem is summarized in Refs. 2-4.

It is instructive to outline three equations:

(1) The viscous equation

$$\left\{ \frac{\partial}{\partial t} + \bar{U}(y) \frac{\partial}{\partial x} - \frac{1}{R_{\delta}} \nabla^2 \right\} \nabla^2 v - \bar{U}_{yy}(y) \frac{\partial v}{\partial x} = 0 \quad (4.1)$$

has a

4th-order derivative in x
4th-order derivative in y
1st-order derivative in t

This equation yields four basic solutions far from the boundary layer: The decaying and growing vortical fluctuations (which propagate downstream and upstream respectively) and the decaying and growing standing waves which are irrotational. The family of eigenmodes vanish far from the wall.

(2) The inviscid form of the above equation

$$\left\{ \frac{\partial}{\partial t} + \bar{U}(y) \frac{\partial}{\partial x} \right\} \nabla^2 v - \bar{U}_{yy}(y) \frac{\partial v}{\partial x} = 0 \quad (4.2)$$

has a

3rd-order derivative in x
2nd-order derivative in y
1st-order derivative in t

Far from the boundary layer, this equation yields only three basic solutions: A nondecaying traveling wave of vorticity (representing vortices being convected downstream), and a pair of decaying and growing standing waves. The solution corresponding to the present work is missing.

(3) The viscous equation for the case of no mean flow reduces to

$$\left\{ \frac{\partial}{\partial t} - \frac{1}{R_0} \nabla^2 \right\} \nabla^2 v = 0 \quad (4.3)$$

and has the same order of derivatives as case (1), with three solutions corresponding to vorticity diffusing downstream and upstream, and two standing waves. In this case, the exponential decay of the two viscous solutions are symmetric; the asymmetry introduced by the mean flow and x-dependence through the term $\bar{U} \partial / \partial x$ is lost. A similar case arises for spanwise fluctuations for the special case of vanishing x-wavenumber.

4.2 SUMMARY OF THE FORMULATION AND NUMERICAL TECHNIQUE

For small-amplitude disturbances in shear layers which develop sufficiently slowly such that the parallel-flow representation is adequate, the objective is to obtain solutions of the equation

$$\left\{ \frac{\partial}{\partial t} + \bar{U}(y) \frac{\partial}{\partial x} - \frac{1}{R_0} \nabla^2 \right\} \nabla^2 v - \bar{U}_{yy}(y) \frac{\partial v}{\partial x} = 0 \quad (4.4)$$

which are of the Fourier-Laplace form

$$v(x, y, z, t) = \phi(y) \exp[i\alpha x + i\gamma z - i\omega t] \quad (4.5)$$

where the frequency ω is real, and the x-wavenumber is complex

$$\alpha = \frac{-iR_0}{2} \left\{ 1 + \left[1 + \frac{4}{R_0^2} (\beta^2 + \gamma^2 - i\omega R_0) \right]^{1/2} \right\} \quad (4.6)$$

The motivations for seeking numerical solutions of this form are that such waves appear in analytical solutions where the mean flow is uniform, as shown in Chapter 1. Furthermore, in an asymptotic analysis of an initial-value problem with a boundary layer, a branch line indicated that waves of this form would exist in boundary layers. For solutions of this form, the equi-phase speed is

$$c_{ep} = \omega/a_T = -1 - 2\epsilon^2(\beta^2 + \gamma^2 + \omega^2) + 2\epsilon^4(\beta^2 + \gamma^2 + \omega^2)(\beta^2 + \gamma^2 + 5\omega^2) + O(\epsilon^6) \quad (4.7)$$

The impermeability and no-slip boundary conditions at the wall, and the boundedness condition of the solution far-away, are

$$\phi = D\phi = 0 \text{ at } y = 0 \text{ and } \phi \text{ is bounded as } y \rightarrow \infty \quad (4.8a,b,c)$$

When $\bar{U} = 1$, the Orr-Sommerfeld equation has the solutions

$$\phi(y) = Ae^{-my} + Be^{+my} + C\cos\beta y + D\sin\beta y \quad (\text{for } y > y_0) \quad (4.9a)$$

or equivalently

$$\phi(y) = Ae^{-my} + Be^{+my} + C_2 \exp(-i\beta y) + D_2 \exp(i\beta y) \quad (\text{for } y > y_0) \quad (4.9b)$$

$$\text{where the exponent is } m = (\alpha^2 + \gamma^2)^{1/2} \quad (4.10)$$

For a boundary layer, $B = 0$. For most cases, solution (4.9a) is normalized by setting $C=1$.

Far-away from the boundary layer edge where the term $A\exp(-my)$ is negligible, the flowfield varies sinusoidally

$$\phi(y) = C\cos\beta y + D\sin\beta y \quad (\text{for } y \gg y_0) \quad (4.11)$$

This freestream disturbance is rotational. The constant D is obtained numerically.

In general, the constants A and D and the solution $\phi(y)$ of the Orr-Sommerfeld equation depend on the frequency, y -wavenumber, Reynolds number, and the mean velocity profile.

Numerical solutions of the Orr-Sommerfeld equation at low Reynolds numbers are obtained by an expansion in a series of (typically 48) Chebyshev polynomials. The coefficients of those polynomials are obtained as solutions of a set of linear, algebraic equations. The matrix of coefficients is reduced by Gauss-Jordan elimination. Calculations are carried out on a Digital Equipment Corporation PDP-11/23 computer using 64K bytes of memory and another 64K bytes of extended memory for virtual arrays. The disk-overlaid FORTRAN IV program executes in about 145 seconds when using the KEF11-AA floating point chip, beginning with data for the mean velocity profile, and ending with the coefficients of the polynomials and the amplitude $\phi(y)$. The program executes in about 80 seconds when accessing the FPF-11 floating point board.

4.3 SUMMARY OF RESULTS, DISCUSSION AND CONCLUSIONS

The analyses and calculations indicate that a very rapidly growing solution of the Orr-Sommerfeld equation exists which differs in form and behavior from the Tollmien-Schlichting wave (the fundamental eigensolution). The wave has the usual Fourier-Laplace form, eqn.(4.5). The oscillation grows very rapidly as $\exp(+R_0 x)$ in the streamwise direction. The solution is a traveling wave which propagates upstream with a speed greater than the freestream speed, U_∞ , i.e. $c_{ep} < -1$. In the inviscid limit, the growth rate becomes infinite. This result reflects the idea that diffusion upstream cannot occur without viscosity. The rapid decay in the upstream direction arises because the vorticity must diffuse upstream against the mean flow. This growing, upstream-traveling wave also differs in form from the growing standing wave of Refs. 13 and 14.

In the uniform mean flow outside of the boundary layer, the solutions oscillate as a superposition of neutral sinusoidal waves, $\cos\beta y$ and $\sin\beta y$, as well as another high-frequency oscillation. Because this high-frequency oscillation may decay very slowly, it can survive into the freestream. In the freestream, this high-frequency oscillation is irrotational. Inside the boundary layer, high-frequency rotational fluctuations are generated.

Since the solutions admit oscillations of the form $\exp(-iR_0 y)$, the calculations have been restricted to low Reynolds numbers where evidence exists of convergence. By increasing the number of terms in the series expansion, and perhaps also the precision of the calculation, higher Reynolds number cases could be calculated. The author notes that the computer program which has calculated Tollmien-Schlichting waves at $R_0=4000$ has only marginal convergence at $R_0=10$ for the present wave with 48 terms in the series expansion. For this reason, the numerical solutions plotted in Chapter 3 are preliminary.

In Refs. 13 and 14, the role of the growing standing wave in numerical solutions of the partial differential equations was discussed. That discussion is repeated below, since the growing, rotational solutions documented in this report will also arise in numerical solutions.

Refs. 17-24 are examples of numerical solutions which have been obtained for unsteady boundary layer problems with finite difference, vortex filament, and spectral techniques. These investigators have been faced with the difficulty of properly posing the boundary conditions on the downstream, outer, and upstream boundaries of the calculational regions. This problem with boundary conditions will become more severe as the disturbances adopt the characteristics of freestream turbulence and its interaction with the leading edge, as the amplitudes increase, and as 3-D and other significant features are included.

The growing vortical wave could be a factor in obtaining numerical solutions in a rectangular domain, since those waves are a mechanism by which the downstream boundary condition can influence the flow elliptically. Improperly formulated boundary conditions can excite extraneous fluctuations in the calculational domain. Numerical errors from roundoff and truncation could grow extremely rapidly if a marching scheme in the downstream direction

were employed and if this solution were excited and uncontrolled. Elimination of these dangerous waves may be necessary.

In other cases as suggested by the paragraphs above, the proper boundary conditions should incorporate vortical waves which naturally enter into the calculational region across the upstream boundary. This wave is a viscous mechanism for upstream communication in this elliptic problem.

Analogous waves also appear in 3-D cases. For at least one of the cases of spanwise fluctuations in a boundary layer, the analogous diffusive wave decays away from a vorticity source much less rapidly than the streamwise case documented here.

REFERENCES

1. Rogler, Harold L. and Reshotko, Eli, "Spatially decaying array of vortices", The Physics of Fluids, vol. 19, no. 12 (December 1976).
2. Tsuge', Shunichi and Rogler, Harold L., "An Asymptotic Solution of the Orr-Sommerfeld Equation Based on a Special Coordinate Stretching", 33rd Annual Meeting of the Fluid Dynamics Division of the American Physical Society, Cornell University, November 1980; Bulletin of the American Physical Society, vol. 25, no. 9 (November 1980).
3. --, "The Two-Dimensional, Viscous Boundary-Value Problem for Fluctuations in Boundary Layers", AIAA-83-0044, AIAA 21st Aerospace Sciences Meeting (10-13 January 1983).
4. --, "The Boundary-Value Problem for Two-Dimensional Fluctuations in Boundary Layers", AEDC TR-84- (September 1984 to appear).
5. Salwen, Harold and Grosch, Chester E., "The continuous spectrum of the Orr-Sommerfeld equation, Part 2. Eigenfunction expansions", J. Fluid Mechanics, vol. 104, pp. 445-465 (1981).
6. Aldoss, T.K. and Reshotko, E. "Contribution of roughness to disturbances in a boundary layer", Bulletin of the American Physical Society, vol. 27, no. 9 (November 1982).
7. Aldoss, T.K., "Initial-value study of effect of distributed roughness on boundary layer transition", Ph.D. dissertation, Case Western Reserve University, Cleveland, Ohio (August 1982).
8. Rogler, Harold L. and Tsuge', Shunichi, "Initial-Value Problem and Solutions for Three-Dimensional Disturbances in Boundary Layers and Free-Shear Layers", 34th Meeting of the American Physical Society, 22-24 November 1981. Bulletin of the American Physical Society, vol. 26, no. 9, (November 1981).
9. Rogler, Harold L., "The production of higher and lower modes and the decay of an array of vortices near a boundary", Bulletin American Physical Society, vol. 20, no. 9 (November 1975).
10. Gustavsson, L. Håken, "Initial-value problem for boundary layer flows", Physics of Fluids, vol. 22, no. 9, pp. 1602-1605 (1979).
11. Rogler, Harold L., "Freestream vorticity disturbances adjusting to the presence of a plate - a quarter-plane problem", J. Applied Mech., vol. 44, no. 4 (December 1977).
12. Mack, Leslie M., "A numerical study of the temporal eigenvalue spectrum of the Blasius layer", J. Fluid Mech., vol. 73 (1976).
13. Rogler, Harold L., "Unsteady, Exponentially-Varying Standing Waves in

NOMENCLATURE

English

a_m	coefficient of the mth Chebyshev polynomial
A, B, C, D	constants in the uniform-flow solution of the Orr-Sommerfeld equation
$c = c_r + ic_i = \omega/a$	complex phase speed
$c_{ep} = \omega/a_r$	equi-phase speed
$D = d/dy$	ordinary derivative in the y-direction
$D^n = d^n/dy^n$	nth ordinary derivative ($D^0 \phi = \phi$)
$E(y) = (\bar{u}^2 + \bar{v}^2)/2$	averaged disturbance kinetic energy per unit mass
$f(y) = f_r + if_i$	complex amplitude of the longitudinal velocity
i	$(-1)^{1/2}$
m	exponent; index on Chebyshev polynomial
N	number of terms in the series expansion
p	disturbance pressure
R_δ	Reynolds number based on characteristic thickness of the boundary layer
t	time
T_m	mth Chebyshev polynomial
u, v, w	disturbance velocities in the x, y and z directions
\bar{U}	mean x-velocity in the streamwise direction
U_∞	mean velocity in the freestream
x	coordinate parallel to plate and in streamwise direction
y	coordinate normal to the plate
y_e	y-value of the boundary layer "edge"
z	lateral or spanwise coordinate
$Z(y) = Z_r + iZ_i$	complex amplitude of the fluctuating vorticity

- Boundary Layers", AIAA-83-0045, AIAA 21st Aerospace Sciences Meeting, Reno, Nevada (10-13 January 1983).
14. --, "Exponentially-varying, unsteady standing waves in parallel-flow boundary layers", AEDC-TR-83-4 (May 1983).
 15. Nachtsheim, Phillip R. and Swigert, Paul, "Satisfaction of asymptotic boundary conditions in numerical solution of systems of nonlinear equations of boundary layer type", NASA E-2959 (1965).
 16. Tsuge', S., "Methods of separation of variables in turbulence theory", NASA CR-3054 (1978).
 17. Ludloff, H.F., De Santo, D.F., and Parthasarathy, R., "Attempts at derivation of transition from laminar into turbulent flow along a flat plate", AFOSR TN 60-105, New York University (January 1960).
 18. Wray, Alan and Hussaini, M.Y., "Numerical Experiments in boundary layer stability", AIAA 18th Aerospace Sciences Meeting (14-16 January 1980).
 19. Leonard, A., "Numerical simulation of interacting, three-dimensional vortex filaments", Lecture Notes in Physics, vol. 35, Springer-Verlag, Berlin (1975).
 20. Grosch, Chester E., "Numerical simulation of instability and transition", Low-Speed Boundary Layer Transition Workshop (16-17 July 1974); Abstract appears in R-1752-ARPA/ONR by William S. King (June 1975).
 21. Fasel, H., "Investigation of the stability of boundary layers by a finite difference model of the Navier Stokes equations", J. Fluid Mech., vol. 78, part 2 (1976).
 22. Miller, G. and A. Callegari, A., "The effects of acoustical disturbances on boundary layer transition", NYU/DAS 78/01, New York University/Dept. of Applied Science, 26-36 Stuyvesant Street (Barney Bldg), New York, New York 10003 (January 1978).
 23. Orszag, S.A., "Turbulence and Transition: A Progress Report", Proceedings of the Fifth International Conference on Numerical Methods in Fluid Dynamics Springer-Verlag, Berlin (1976).
 24. Murdock, John W., "Tollmien-Schlichting waves generated by unsteady flow over parabolic cylinders", Paper-AIAA-81-0199, AIAA 19th Aerospace Sciences Meeting (12-15 January 1981).

Greek and Script

α	x-wavenumber
β	y-wavenumber
γ	z-wavenumber
∇^2	$\partial^2/\partial x^2 + \partial^2/\partial y^2 + \partial^2/\partial z^2$ 3-D Laplacian operator
δ	characteristic thickness of the boundary layer
$\epsilon = 1/R_\delta$	inverse of Reynolds number
η	$(2y/y_e) - 1$
ν	kinematic viscosity
ξ	disturbance vorticity in the z-direction
$\pi(y) = \pi_r + i\pi_i$	complex amplitude of pressure disturbance
$\theta(y) = \theta_r + i\theta_i$	complex amplitude of the normal velocity disturbance
ψ	streamfunction
ω	frequency

Superscripts, Subscripts, and Miscellaneous Notation

$\overline{(\quad)}$	the time average over one time period
e	boundary layer edge
r, i	real and imaginary parts of a complex variable
$(\quad)_x$	partial derivative with respect to x
$\hat{\hat{\quad}}$	double generalized Fourier transform

END

FILMED

10-85

DTIC